


Converting a triplet Cooper pair supercurrent into a spin signal

Sigrid Aunsmo  and Jacob Linder 

Center for Quantum Spintronics, Department of Physics, Norwegian University of Science and Technology, NO-7491 Trondheim, Norway

 (Received 12 August 2023; revised 1 December 2023; accepted 4 December 2023; published 4 January 2024)

Superconductivity with spin-polarized Cooper pairs is known to emerge by combining conventional spinless superconductors with materials that have spin-dependent interactions, such as magnetism and spin-orbit coupling. This enables a dissipationless and conserved flow of spin. However, actually utilizing the spin polarization of such supercurrents has proven challenging. Here, we predict an experimental signature of current-carrying triplet Cooper pairs in the form of an induced spin signal. We show that a supercurrent carried only by triplet Cooper pairs induces a nonlocal magnetization that is controlled by the polarization direction of the triplet Cooper pairs. This provides a measurement protocol to directly use the spin polarization of the triplet Cooper pairs in supercurrents to transfer spin information in a dissipationless manner.

DOI: [10.1103/PhysRevB.109.024503](https://doi.org/10.1103/PhysRevB.109.024503)

I. INTRODUCTION

Substantial efforts have been made to find evidence of dissipationless currents carried by spin-polarized Cooper pairs in superconductors [1,2], also referred to as triplet Cooper pairs. This includes measurements of how Gilbert damping is renormalized in Josephson junctions and superconducting bilayers subject to ferromagnetic resonance [3–8], as well as long-ranged supercurrent flow through magnetic materials [9–11]. Spin pumping in ferromagnet/superconductor (FM/S) hybrid structures [12,13], where triplet pairing will affect the spin accumulation in the superconductor, has recently been the subject of increased theoretical interest [14–21].

However, a long-ranged supercurrent through magnetic materials is in itself not necessarily useful. Supercurrents through normal metals carried by spinless, singlet Cooper pairs are also long ranged when flowing through a normal metal. Thus, to unlock the potential of spin-polarized supercurrents with regard to potential cryogenic devices, it is necessary to find a way to utilize their spin polarization directly. We here predict that a supercurrent carried by spin-polarized Cooper pairs induces a nonlocal magnetization. Both the polarization direction and magnitude of this magnetization are directly controlled by the spin degree of freedom of the triplet Cooper pairs. This shows how spin supercurrents can be used for low-dissipation information transfer by inducing spin signals.

The supercurrent flow is converted into a nonlocal magnetization, occurring in a region where the supercurrent does not flow, by allowing it to interact with a Rashba spin-orbit coupled interface. This can be probed in the setup shown in Fig. 1. We consider the scenario experimentally realized in, e.g., Refs. [10,11]: a spin-triplet charge supercurrent generated by a magnetic multilayered structure. In the experiments, the spin-polarized nature of the Cooper pairs carrying the current was not directly measured, but rather inferred from its slow decay as a function of the length of the ferromagnetic bridge in a Josephson junction. In contrast, we provide a way to directly convert the spin of the triplet supercurrent into a

spin signal. The induced magnetization \mathbf{M} in the normal metal (N) changes direction depending on the spin polarization of triplet pairs carrying the supercurrent. Without current, the nonlocal magnetization vanishes. The induced magnetization \mathbf{M} vanishes for certain spin-polarization directions of the pairs relative to the Rashba interface normal. The predicted effect provides a way to directly use the spin polarization of the triplet Cooper pairs in supercurrents to transfer spin information in a dissipationless manner.

II. THEORY

The quasiclassical theory of superconductivity [22–24] is documented to compare well with experimental results, even quantitatively, for measurements performed in mesoscopic superconducting hybrid structures. Our starting point is the Usadel equation, which can be used in the diffusive limit of transport where the length scale hierarchy $\lambda_F \ll l_{\text{mfp}} \ll \xi$ applies, with λ_F being the Fermi wavelength, l_{mfp} being the electronic mean free path, and ξ being the superconducting coherence length. It is effectively an equation of motion for the Green's function matrix \check{g} in Keldysh space and takes the form

$$D\nabla(\check{g}\nabla\check{g}) + i[E\hat{\rho}_3 + \hat{\mathbf{h}} + \hat{\Delta}, \check{g}] = 0. \quad (1)$$

Here, D is the diffusion coefficient, E is the quasiparticle energy, $\hat{\mathbf{h}} = \text{diag}(\mathbf{h} \cdot \boldsymbol{\tau}, \mathbf{h} \cdot \boldsymbol{\tau}^*)$, where \mathbf{h} describes the spin-splitting field, $\boldsymbol{\tau}$ is a vector with Pauli matrices as its components, $\hat{\rho}_3 = \text{diag}(1, 1, -1, -1)$, and $\hat{\Delta} = \begin{pmatrix} 0 & i\sigma_y\Delta \\ -i\sigma_y\Delta^* & 0 \end{pmatrix}$ describes the effect of the complex superconducting order parameter Δ . The quasiclassical Green's function \check{g} is an 8×8 matrix in Keldysh space and thus has retarded, advanced, and Keldysh components [25]. We have used the spinor basis $[\psi_\uparrow(\mathbf{r}), \psi_\downarrow(\mathbf{r}), \psi_\uparrow^\dagger(\mathbf{r}), \psi_\downarrow^\dagger(\mathbf{r})]$ when defining the Green's function matrices. Since we will consider a system in equilibrium, \check{g} is entirely determined by the retarded Green's function \hat{g} , which is a 4×4 matrix in Nambu-spin space. This retarded Green's function depends on both the normal Green's function

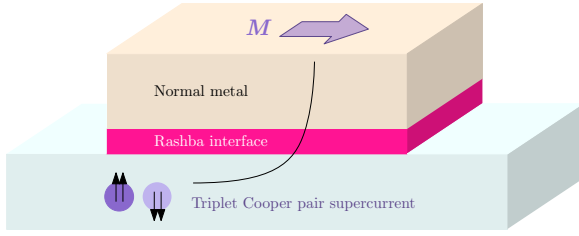


FIG. 1. Sketch of the proposed experimental protocol for converting a supercurrent carried by spin-polarized triplet Cooper pairs into a nonlocal spin signal. The supercurrent flows in a region underneath a thin heavy metal layer. Due to interfacial Rashba spin-orbit coupling, the triplet pairs induce a magnetization in a normal metal where no supercurrent is flowing. The induced magnetization depends sensitively on the polarization direction of the triplet pairs.

g , which is a 2×2 matrix in spin space determining spectral properties such as the density of states, and the anomalous Green's function f , which contains information about the superconducting correlations. The appearance of 4×4 matrices in an equation with 8×8 matrices, such as Eq. (1), should be understood as a repeated matrix on the diagonal. In effect, in places where the dimensions of matrices multiplied together are inconsistent, Kronecker products with the necessary identity matrices are implied for the matrix with the lower dimensionality.

To solve this equation, it needs to be complemented by boundary conditions. In our system, we will have both magnetic and spin-orbit coupled interfaces. For the magnetic (also referred to as spin-active) interfaces we have [1,26,27]

$$\hat{g}_L \partial_z \hat{g}_L = G_0 [\hat{g}_L, \hat{g}_R] + G_1 [\hat{g}_L, \hat{m} \hat{g}_R \hat{m}] + G_{MR} [\hat{g}_L, \{\hat{g}_R, \hat{m}\}] - iG_\phi [\hat{g}_L, \hat{m}]. \quad (2)$$

Here, $\hat{m} = \text{diag}(\mathbf{m} \cdot \boldsymbol{\tau}, \mathbf{m} \cdot \boldsymbol{\tau}^*)$, where \mathbf{m} is a unit vector that describes the interface magnetization, G_0 describes the ratio between the barrier resistance and the normal-state resistance of material L , G_{MR} describes the magnetoresistance effect of the interface, and G_1 originates from the spin-dependent transmission probabilities of spin-active interfaces. The conductance parameters G_1 and G_{MR} can be written in terms of the normal-state transmission probability T_n and spin polarization P_n associated with each scattering channel n for the interface. Here, we assume for simplicity that each scattering channel has the same polarization $P = P_n$, in which case one obtains [1]

$$\frac{G_1}{G_0} = \frac{1 - R_P}{1 + R_P}, \quad \frac{G_{MR}}{G_0} = \frac{P}{1 + R_P}, \quad (3)$$

with $R_P = \sqrt{1 - P^2}$. Finally, G_ϕ describes the effect of quasiparticles picking up spin-dependent phase shifts as they scatter at the interface. The boundary conditions for \hat{g}_R are obtained by interchanging L and R and multiplying the entire right-hand side by -1 . For an in-depth discussion and derivation of these boundary conditions, see Refs. [1,26,27]. We will also need the boundary conditions for a spin-orbit coupled interface [28,29]. Defining $\boldsymbol{\tau}_\parallel = (\rho_x, 0, \rho_z)$,

these read

$$\begin{aligned} D\check{g}_R \partial_y \check{g}_R &= T_0^2 [\check{g}_L, \check{g}_R] - \frac{2}{3} T_1^2 p_F^2 [\check{g}_R, \boldsymbol{\tau}_\parallel \check{g}_L \boldsymbol{\tau}_\parallel] \\ &\quad - mDT_0 T_1 [\check{g}_R, \{\boldsymbol{\tau}_\parallel, x, \check{g}_L \partial_z \check{g}_L\}] \\ &\quad + Dd\alpha^2 [\rho_x, \check{g}_R \rho_x \check{g}_R] + Dd\alpha^2 [\rho_z, \check{g}_R \rho_z \check{g}_R], \quad (4) \end{aligned}$$

where T_0 and T_1 are phenomenological interface parameters describing, respectively, spin-independent tunneling and spin-flip tunneling induced by the interfacial Rashba spin-orbit coupling, m is the electron mass, p_F is the Fermi momentum, α quantifies the spin-orbit coupling strength, and d is the thickness of the spin-orbit coupled interface.

III. OBSERVABLES

Our primary goal is to determine how triplet Cooper pair supercurrents can induce a magnetization in a normal metal by scattering on a spin-orbit coupled interface. To do so, we need the expressions for magnetization and current in quasiclassical theory. In this section, the quasiclassical expressions for the magnetization as well as spin and charge currents are presented. To simplify the analytical study later on, we also present the observables expressed in the singlet-triplet decomposition in the weak-proximity-effect regime.

A. Currents

The quasiclassical expression for current can be found by using the continuity equation $\partial_t \rho + \nabla \cdot \mathbf{j} = S$, where \mathbf{j} is the current of a quantity, S is any source term present, and ρ is the density of the quantity such as charge or spin. In a normal metal, the source term vanishes for the charge current.

For charge, we have that the density can be written as $\rho = e \langle \psi^\dagger \hat{\rho}_3 \psi \rangle$, and for spin the spin density can be written as $\langle \psi^\dagger \frac{1}{2} \hat{\rho}_3 \boldsymbol{\tau} \psi \rangle$, where $e < 0$ is the electron charge and we set $\hbar = 1$. By using the Heisenberg equation of motion for the creation and annihilation operators ψ^\dagger , ψ and writing the expression in terms of the quasiclassical expression we get for the charge current density [30,31]

$$\mathbf{J} = \frac{eN_0 D}{4} \int dE \text{Tr} [\hat{\rho}_3 (\check{g} \bar{\nabla} \check{g})^K]. \quad (5)$$

The spin current density is a tensor, with a direction of flow in real space and a polarization direction in spin space, obtained by replacing $\hat{\rho}_3$ with $\frac{1}{2} \hat{\rho}_3 \boldsymbol{\tau}$.

As mentioned, we will write the expressions in terms of the singlet-triplet decomposition terms f_s and \mathbf{d} : $f = (f_s + \mathbf{d} \cdot \boldsymbol{\sigma}) i\sigma_y$. By linearizing in \hat{f} , assuming $\hat{g} = \hat{\rho}_3 + \hat{f}$, and using the relation $\hat{g}^A = -\hat{\rho}_3 (\hat{g}^R)^\dagger \hat{\rho}_3$ and the fact that in equilibrium we have $\hat{g}^K = (\hat{g}^R - \hat{g}^A) \tanh(\frac{\beta E}{2})$ we get the following expressions for the current density \mathbf{J} and spin current density \mathbf{J}_s :

$$\begin{aligned} \mathbf{J} &= J_0 \int_0^\infty \frac{dE}{\Delta_0} \xi \tanh\left(\frac{\beta E}{2}\right) \text{Re}([f_s \nabla \tilde{f}_s - d_z \nabla \tilde{d}_z \\ &\quad - d_x \nabla \tilde{d}_x - d_y \nabla \tilde{d}_y] - [\cdot \tilde{\cdot}]), \quad (6) \end{aligned}$$

$$\mathbf{J}_s = J_{s0} \int_0^\infty \frac{dE}{\Delta_0} \xi \tanh\left(\frac{\beta E}{2}\right) \text{Im}([d_y \nabla \tilde{d}_z - d_z \nabla \tilde{d}_y] + [\cdot \tilde{\cdot}]), \quad (7)$$

$$\mathbf{J}_{s_y} = J_{s0} \int_0^\infty \frac{dE}{\Delta_0} \xi \tanh\left(\frac{\beta E}{2}\right) \text{Im}([d_z \nabla \tilde{d}_x - d_x \nabla \tilde{d}_z] + [\cdot \tilde{\cdot}]), \quad (8)$$

$$\mathbf{J}_{s_z} = J_{s0} \int_0^\infty \frac{dE}{\Delta_0} \xi \tanh\left(\frac{\beta E}{2}\right) \text{Im}([d_x \nabla \tilde{d}_y - d_y \nabla \tilde{d}_x] + [\cdot \tilde{\cdot}]), \quad (9)$$

where $J_0 = 2eN_0 D \Delta_0 / \xi$ and $J_{s0} = N_0 D \Delta_0 / \xi$. We have written the integral in terms of the dimensionless variable E / Δ_0 , where $\Delta_0 = \Delta(T = 0)$ is the zero-temperature energy gap, and the dimensionless spatial coordinate z / ξ . This means that J / J_0 are now dimensionless and can be used in the numerical study.

In the following sections, we will also use the charge current divided into which component carries the current. Therefore we introduce the notation

$$\mathbf{J}_{f_s} = J_0 \int_0^\infty \frac{dE}{\Delta_0} \tanh\left(\frac{\beta E}{2}\right) \text{Re}([f_s \nabla \tilde{f}_s] - [\cdot \tilde{\cdot}]), \quad (10)$$

$$\mathbf{J}_{d_i} = -J_0 \int_0^\infty \frac{dE}{\Delta_0} \tanh\left(\frac{\beta E}{2}\right) \text{Re}([d_i \nabla \tilde{d}_i] - [\cdot \tilde{\cdot}]), \quad (11)$$

where \mathbf{J}_{f_s} is the charge current carried by the singlet component and \mathbf{J}_{d_i} is carried by the d_i component.

B. Magnetization

The quasiclassical expression for magnetization reads [31]

$$\mathbf{M} = \frac{g\mu_B N_0}{8} \int dE \text{Tr}(\hat{\tau} \hat{g}^K), \quad (12)$$

where g is the Landé g -factor, N_0 is the normal-state density of states at the Fermi level, and μ_B is the Bohr magneton. It should be mentioned that this expression does not take into account the contribution from the entire Fermi sea and is thus not suitable to compute the magnetization of a ferromagnetic metal. It is, on the other hand, suitable for computing any spin magnetization arising in otherwise nonmagnetic materials such as normal metals or conventional superconductors. This holds both for spin accumulations in nonequilibrium systems and proximity-induced equilibrium spin magnetizations.

Once more we want to express the magnetization in terms of the singlet-triplet-decomposed components. This can be done similarly to the current, by using the expression for \hat{g}^A and the equilibrium expression for \hat{g}^K . There are no first-order contributions in the anomalous Green's function; so we have to take into account the normalization condition, $(\hat{g}^R)^2 = 1$. By this method, it can be shown that the magnetization, to the second order in the anomalous Green's function, reads

$$M_x = M_0 \int_0^\infty \frac{dE}{\Delta_0} \tanh\left(\frac{\beta E}{2}\right) \text{Re}(\tilde{d}_x f_s - d_x \tilde{f}_s), \quad (13)$$

$$M_y = M_0 \int_0^\infty \frac{dE}{\Delta_0} \tanh\left(\frac{\beta E}{2}\right) \text{Re}(\tilde{d}_y f_s - d_y \tilde{f}_s), \quad (14)$$

$$M_z = M_0 \int_0^\infty \frac{dE}{\Delta_0} \tanh\left(\frac{\beta E}{2}\right) \text{Re}(\tilde{d}_z f_s - d_z \tilde{f}_s), \quad (15)$$

where $M_0 = g\mu_B N_0 \Delta_0$.

IV. RICCATI PARAMETRIZATION

One particularly convenient way to parametrize the Green's function is the Riccati parametrization [32–35]. The Riccati parametrization is advantageous for numerical computation because the parameters are bounded between 0 and 1. For the purpose of studying systems numerically we will here briefly outline the derivation of the Riccati-parametrized Usadel equation as well as giving a detailed derivation of the Riccati-parametrized boundary equation in Appendixes A and B, including the effect of a spin-orbit coupled interface, since the latter is not present in the existing literature.

The retarded Green's function is defined via parameters N and γ as follows:

$$\hat{g} = \begin{pmatrix} N(1 + \gamma\tilde{\gamma}) & 2N\gamma \\ -\tilde{N}\tilde{\gamma} & -\tilde{N}(1 + \tilde{\gamma}\gamma) \end{pmatrix}. \quad (16)$$

N and γ will only be used for 2×2 matrices; so we do not use any special notation to indicate their matrix nature. By the normalization condition $\hat{g}^2 = 1$ it is seen that $N = (1 - \gamma\tilde{\gamma})^{-1}$ and $\tilde{N} = (1 - \tilde{\gamma}\gamma)^{-1}$.

A couple of useful identities can be found:

$$N\gamma = \gamma\tilde{N}, \quad \tilde{N}\tilde{\gamma} = \tilde{\gamma}N. \quad (17)$$

Notice also that

$$\gamma\tilde{\gamma} = 1 - N^{-1}. \quad (18)$$

When writing the Usadel equation and the boundary conditions, in particular including the role of spin-orbit coupling, we will have to deal with derivatives. To simplify the notation, we therefore introduce $\gamma' = \partial_z \gamma$. The following way of writing derivatives will also be useful:

$$\partial_z N = N(\gamma'\tilde{\gamma} + \gamma\tilde{\gamma}')N, \quad (19)$$

$$\partial_z \tilde{N} = \tilde{N}(\tilde{\gamma}'\gamma + \tilde{\gamma}\gamma')\tilde{N}, \quad (20)$$

$$\partial_z(N\gamma) = N(\gamma' + \gamma\tilde{\gamma}'\gamma)\tilde{N}, \quad (21)$$

$$\partial_z(\tilde{N}\tilde{\gamma}) = \tilde{N}(\tilde{\gamma}' + \tilde{\gamma}\gamma'\tilde{\gamma})N, \quad (22)$$

all of which can be found by using the identities above.

The general approach for identifying the Riccati-parametrized Usadel equations and the Kuprianov-Lukichev boundary conditions is thoroughly described in Ref. [35]. The method consists of writing the terms in the Usadel equation in 4×4 matrix notation and then taking the upper right 2×2 matrix minus the upper left 2×2 matrix multiplied by γ . More specifically, one takes $\frac{1}{2}N^{-1}([\cdot \cdot]_{12} - [\cdot \cdot]_{11}\gamma)$ of the matrix equation $[\cdot \cdot]$, where the subscript indicates a block matrix. Doing so, one manages to eliminate terms such that $\partial_z^2 \gamma$ or $\partial_z \gamma$ terms can be separated out.

The final result for the Riccati-parametrized Usadel equation for a ferromagnet reads

$$\partial_z^2 \gamma = -2iE\gamma - \mathbf{i}\mathbf{h} \cdot (\tau\gamma - \gamma\tau^*) - 2\gamma'\tilde{N}\tilde{\gamma}\gamma', \quad (23)$$

where for a normal metal the only adjustment needed is to set $\mathbf{h} = 0$. It can be shown that the Riccati-parametrized bulk

BCS singlet superconductor solution is

$$\gamma_{\text{BCS}} = \begin{pmatrix} 0 & be^{i\phi} \\ -be^{i\phi} & 0 \end{pmatrix}, \quad (24)$$

where ϕ is the phase and

$$b = \begin{cases} \frac{\Delta}{E+i\sqrt{\Delta^2-E^2}} & \text{for } |E| < \Delta \\ \frac{\Delta \operatorname{sgn}(E)}{|E|+\sqrt{E^2-\Delta^2}} & \text{for } |E| > \Delta. \end{cases} \quad (25)$$

Riccati parametrization of boundary conditions

When deriving the Riccati parametrization of the specific boundary conditions used in this paper, it is useful to note that many of the terms both in the spin-orbit coupling and spin-active boundary conditions have the same form. Here a practical method for Riccati-parametrizing terms of this type is presented in order to simplify the calculations.

The form which many of the terms take is

$$[\hat{g}_L, \hat{U}], \quad (26)$$

where \hat{U} is a matrix whose exact form depends on the specific boundary conditions. In general, we write \hat{U} as

$$\hat{U} = \begin{pmatrix} U_{11} & U_{12} \\ U_{21} & U_{22} \end{pmatrix}. \quad (27)$$

By Riccati parametrization, it can be found from the left-hand side of the boundary equation $\hat{g}\partial_z\hat{g}$ that

$$\frac{1}{2}N_L^{-1}([\hat{g}_L\partial_z\hat{g}_L]_{12} - [\hat{g}_L\partial_z\hat{g}_L]_{11}\gamma_L) = \partial_z\gamma_L, \quad (28)$$

as seen in Ref. [35]. The subscript indicates the block of the matrix that is meant, as in Eq. (27).

To obtain the complete boundary conditions, we have to perform the same operation on the right-hand side as on the left side. This means we need to take $\frac{1}{2}N_L^{-1}([\cdot\cdot]_{12} - [\cdot\cdot]_{11}\gamma_L)$ of every term on the right-hand side of the boundary conditions. Thus we start by finding a procedure for all terms that come in the form of Eq. (26):

$$\begin{aligned} & \frac{1}{2}N_L^{-1}([\hat{g}_L, \hat{U}]_{12} - [\hat{g}_L, \hat{U}]_{11}\gamma_L) \\ &= \frac{1}{2}N_L^{-1}(g_L U_{12} + \underline{f}_L U_{22} - U_{11}\underline{f}_L + U_{12}\tilde{g}_L \\ & \quad - (g_L U_{11} + \underline{f}_L U_{21} - U_{11}g_L + U_{12}\tilde{f}_L)\gamma_L). \end{aligned} \quad (29)$$

As a next step we collect the terms with the same U_{ij} matrices and insert $\underline{f} = 2N\gamma$, $\underline{g} = 2N - 1$. The U_{11} term can be written as

$$\begin{aligned} & \frac{1}{2}N_L^{-1}(-U_{11}\underline{f}_L - g_L U_{11}\gamma_L + U_{11}g_L\gamma_L) \\ &= \frac{1}{2}N_L^{-1}(-U_{11}2N_L\gamma_L - (2N_L - 1)U_{11}\gamma_L \\ & \quad + U_{11}(2N_L - 1)\gamma_L) = -U_{11}\gamma_L. \end{aligned} \quad (30)$$

In the same manner the \hat{U}_{12} term becomes

$$\begin{aligned} & \frac{1}{2}N_L^{-1}(g_L U_{12} + U_{12}\tilde{g}_L - U_{12}\tilde{f}_L\gamma_L) \\ &= \frac{1}{2}N_L^{-1}((2N_L - 1)U_{12} + U_{12}(2\tilde{N}_L - 1) - U_{12}2\tilde{N}_L\tilde{\gamma}_L\gamma_L) \\ &= U_{12}. \end{aligned} \quad (31)$$

The \hat{U}_{21} term should also be written in terms of γ as

$$\frac{1}{2}N_L^{-1}(-\underline{f}_L U_{21}\gamma_L) = -\gamma_L U_{21}\gamma_L. \quad (32)$$

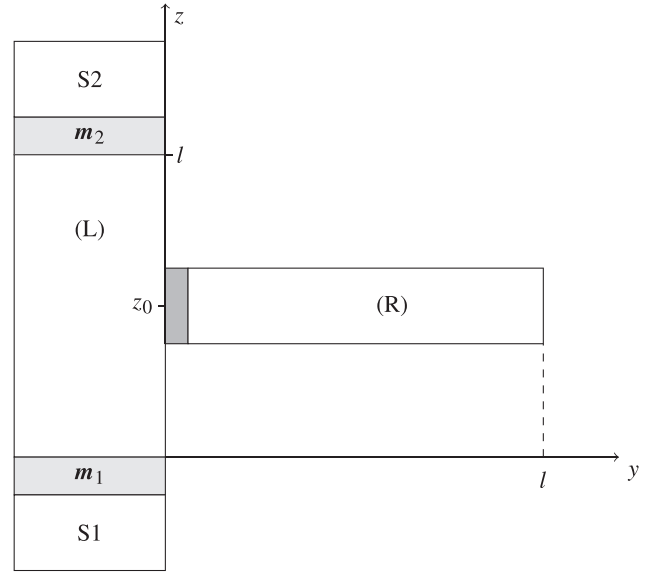


FIG. 2. The system in which supercurrents and induced magnetization are investigated. The material to the left, (L), is the material in which the supercurrent will flow. This material will be either a ferromagnet or a normal metal. To get the current flowing, two conventional superconductors are connected to (L), and a phase difference between them is applied. In between the superconductors and (L), spin-active interfaces are included for the purpose of creating triplet Cooper pairs and thereby also triplet supercurrents. A normal metal, (R), is connected to (L) through a spin-orbit coupled interface. This material borders a vacuum at $y = l$.

Finally, the U_{22} term can be written as

$$\frac{1}{2}N_L^{-1}(\underline{f}_L U_{22}) = \gamma_L U_{22}. \quad (33)$$

Putting everything together, we get

$$\begin{aligned} & \frac{1}{2}N_L^{-1}([g_L, U]_{12} - [g_L, U]_{11}\gamma_L) \\ &= -U_{11}\gamma_L + U_{12} - \gamma_L U_{21}\gamma_L + \gamma_L U_{22}. \end{aligned} \quad (34)$$

We note that this also can be used for the Kuprianov-Lukichev boundary conditions [36], where one would have $\hat{U} = G_0\hat{g}_R$. From this, and using the identities in Eqs. (17) and (18), the Kuprianov-Lukichev boundary conditions can be found to be

$$\partial_z\gamma_L = G_0(1 - \gamma_L\tilde{\gamma}_R)N_R(\gamma_R - \gamma_L), \quad (35)$$

$$\partial_z\gamma_R = G_0(1 - \gamma_R\tilde{\gamma}_L)N_L(\gamma_R - \gamma_L). \quad (36)$$

In Appendixes A and B, both the spin-orbit coupling and spin-active boundary conditions will be written in the Riccati-parametrized form using the method described here.

V. SETUP

The system we are studying is illustrated in Fig. 2. The region in which the supercurrents will flow is drawn to the left and will therefore be referred to as (L). Similarly, the region where induced magnetization will be studied is drawn to the right and is called (R). In this paper, we let the region (R) be a normal metal, and (L) will either be a normal metal or a ferromagnet depending on the situation. The z position

where (R) is connected to (L) is called z_0 . In most situations, we use $z_0 = l/2$, and it will be specified when other values are used. The (L) and (R) regions are chosen to have the same length, but this is not required for the effects predicted here. The gray region between (L) and (R) is the spin-orbit coupled material, for which the spin-orbit coupling boundary conditions will be used. At $z = 0$ and $z = l$, conventional BCS superconductors, S1 and S2, are attached to the (L) material. These superconductors are the sources for Cooper pairs in the rest of the system. Between (L) and the superconductor, spin-active interfaces are introduced and are marked as gray regions in the figure. The interface magnetizations of the spin-active interfaces are described by unit vectors \mathbf{m}_1 and \mathbf{m}_2 .

To create a pure singlet charge current, the interface magnetizations are switched off ($\mathbf{m}_1 = \mathbf{m}_2 = 0$), which is equivalent to using the regular Kuprianov-Lukichev boundary conditions. Furthermore, (L) is a normal metal in the singlet current case. As the superconductors S1 and S2 only contain singlet Cooper pairs, no triplets will be induced in (L) in this scenario. We want a supercurrent to flow through the (L) region. This is achieved by applying a phase difference, ϕ , between S1 and S2.

To create the triplet charge current and the spin current, the interface magnetizations are switched on. The triplet charge current is created in the same way as in the singlet case: by applying a phase difference.

For the purpose of discovering effects caused solely by triplets, a ferromagnetic exchange field is included in the material (L). Because of the exchange field, the singlet becomes short ranged and dies out rapidly in the (L) region. In an experimental setup, it would be of importance to separate the intrinsic magnetization coming from an exchange field and the magnetization induced by supercurrents. Therefore the exchange field is modeled to be spatially varying in (L) such that it is zero in the middle region but large at the sides (as shown later in Fig. 4). In practice, this can be realized by attaching thin ferromagnetic regions with a strong exchange field right next to the superconductors and then having a long normal metal region separating the ferromagnets. In this way, the singlets and short-range triplets are filtered out by the thin, strongly polarized ferromagnetic regions, whereas the long-range triplets produced in the ferromagnetic region remain and can propagate through the normal metal. More specifically, it is the triplet component that is spin neutral in the exchange field orientation $\mathbf{d} \parallel \mathbf{h}$ that is short ranged, and the others are long ranged.

As we will discuss in the following analytical study, the difference between the d_z and d_y components is quite insignificant relative to the spin-orbit coupled interface, and it is instead the d_x component that is the most relevant. Therefore we focus most of the discussion on the case where the interface magnetizations lie in the xy plane and the exchange field points in the z direction, $\mathbf{h} = (0, 0, h(z))$. We do, however, include rotation of both \mathbf{m}_1 and \mathbf{m}_2 with an angle α around the z axis, and the angle between \mathbf{m}_1 and \mathbf{m}_2 which we call θ . These angles are illustrated in Fig. 3. We also note here that the directions chosen are advantageous for an experimental setup, as rotating the interface magnetizations in plane is a simpler task than driving them out of the xy plane.

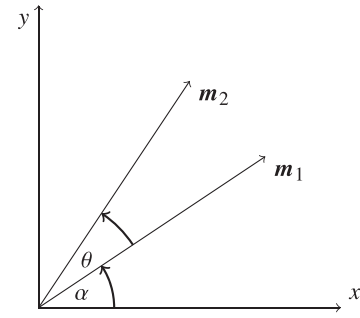


FIG. 3. Definition of the angles α and θ . α is defined as the angle between the x axis and the interface magnetization of the first interface, \mathbf{m}_1 . θ is the angle between the two interface magnetizations.

We also remark that rotating both interface magnetizations, \mathbf{m}_1 and \mathbf{m}_2 , by an angle α is equivalent to rotating material (L) around the z axis. Thus, rotating the interface magnetization or attaching the (R) region to the (R) region at different angles corresponds to the same physical system.

In the numerical study, we have used the interface parameters $\frac{T_0^2}{D} = 0.2/\xi_s$, $\frac{2}{3} \frac{T_1^2 P^2}{D} = mT_0 T_1 / \xi_s = d\alpha^2 = 0.1/\xi_s$, unless specified otherwise. To create pure charge currents, we set $P = 0$ and $G_\phi = 3G_0$. We also checked that the results are qualitatively similar if one instead uses $P \neq 0$, $G_\phi = 0$. If both P and G_ϕ are finite, spin supercurrents in addition to charge supercurrents flow in the system. Furthermore, a combination of a length of material (L), l , that is short enough to preserve some of the triplets and a strength of \mathbf{h} that is strong enough to remove the singlet had to be found. Setting the length of the material, l , to eight times the bulk superconducting coherence length, $l = 8\xi_s = 8\sqrt{D/\Delta_0}$, and $h(z)$ as in Fig. 4 was found to work well.

Finally, we emphasize that our main aim here is to determine the qualitative behavior of the spin signal induced by the charge and spin currents, such as when it exists and how it changes depending on the polarization of the triplet Cooper

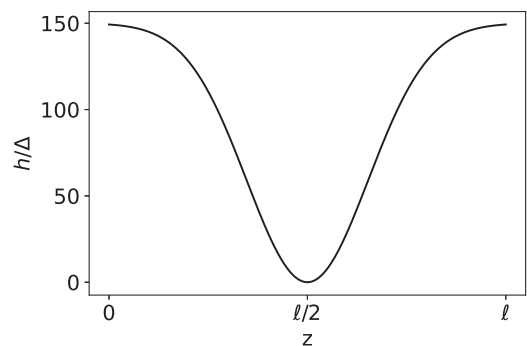


FIG. 4. The spatial profile of the exchange field function $h(z)$ which is applied to the left material (L) in the triplet current cases. This ensures that only the long-ranged triplet component survives at the contact with the normal metal through the Rashba spin-orbit coupled interface. In an experiment, one would use a strong ferromagnet/normal metal bilayer to achieve an exchange field spatial profile serving the same purpose. In this paper, the spatial profile of h is continuous rather than abrupt for numerical convenience, as one can then evaluate the Usadel equation in a single layer.

pairs, and not predict its precise magnitude, which will depend on the material choices.

Numerical method

In general, the materials on both sides of an interface are affected by each other. However, here it is assumed for simplicity that the inverse proximity effect that material (L) induces in S1 and S2 is negligible, and only the effect from the superconductor on the material (L) is considered. The superconductors are thus assumed to be the bulk superconductors. Such an approximation is valid when one of the materials is much more disordered than the other [37]. The bulk superconductor Green's function can by this assumption be used directly in the boundary conditions used to solve system (L). Similarly, the effect from (R) on (L) is neglected, and the solution for system (L) at $z = z_0$ is used directly in the spin-orbit coupling boundary conditions for (R). Furthermore, the materials are individually modeled as one dimensional, meaning that material (L) is extended in the z direction and (R) is extended in the y direction.

The system which has to be solved is now the one-dimensional Usadel equation in two regions. This is a second-order differential equation for two variables, γ and $\tilde{\gamma}$, and to solve it numerically we rewrite it as four first-order differential equations writing

$$\begin{pmatrix} \gamma' \\ \gamma'' \\ \tilde{\gamma}' \\ \tilde{\gamma}'' \end{pmatrix} = f \begin{pmatrix} \gamma \\ \gamma' \\ \tilde{\gamma} \\ \tilde{\gamma}' \end{pmatrix}, \quad (37)$$

where $f(\dots)$ is a function that returns the derivative of the input. The function will thus return γ' as the derivative for γ and use the Riccati-parametrized Usadel equation to find the derivative of γ' and similarly for $\tilde{\gamma}$. Thus we have a system of 16 complex connected differential equations, four elements in each of the matrices γ , γ' , $\tilde{\gamma}$, and $\tilde{\gamma}'$. The boundary conditions give restrictions to γ' and $\tilde{\gamma}'$ on each side of the material.

To solve the system, we have used the boundary value problem solver from SCIPY [38]. To stabilize the solver, the real and imaginary parts are split such that the 16 complex equations become 32 real ones. To increase numerical stability, inelastic scattering is also included by adding a small imaginary component to the energy, which here is set to $\delta/\Delta_0 = 0.01$ as used in Ref. [39]. This imaginary component is referred to as the Dynes parameter and is often used to model experiments [40]. In essence, it has the effect of broadening the spectral features, such as the peaks of the Green's functions that occur at $E = 0$ and $E = \Delta$. As mentioned, the interface magnetizations are rotated in the xy plane in the triplet cases. A small trick was used to solve the system with these rotations. To save computation time, the Usadel equation only has to be solved once in material (L) for one given θ and one given set of interface parameters. The angle α can simply be taken into account by rotating the triplet components $d_{x,L}$ and $d_{y,L}$, such that

$$\begin{aligned} d_{x,L}(\alpha) &= d_{x,L}(0) \cos(\alpha) + d_{y,L}(0) \sin(\alpha), \\ d_{y,L}(\alpha) &= -d_{x,L}(0) \sin(\alpha) + d_{y,L}(0) \cos(\alpha). \end{aligned} \quad (38)$$

This means that instead of solving the system in (L) for every α , we solve it once and then rotate the solution to proceed studying the material (R). For the material (R), however, the Usadel equation needs to be solved separately for every value of α . We have verified the integrity of our numerical method by, e.g., checking that current conservation is satisfied and that we reproduce known results from the literature, such as the induced magnetization from a singlet charge current in Ref. [29].

VI. A BRIEF ANALYTICAL STUDY

To gain more physical insight before proceeding to the numerical results, we here analyze the weak-proximity-effect regime where the equations can be linearized in the anomalous Green's function. We will see that there is a clear relation between the singlet charge current, J_{f_s} , and the induced magnetization in the x direction, m_x . A similar relation also exists between a triplet charge current carried by the d_x triplet, J_{d_x} , and m_x .

In the weak-proximity-effect regime, we assume that the quasiclassical Green's function is close to the normal metal solution, $\hat{g}_N = \hat{\rho}_3$, but with a small superconducting part, \hat{f} , induced by the proximity superconductors. We thereby assume that we can use the weak-proximity-effect solution $\hat{g} \approx \hat{\rho}_3 + \hat{f}$. Using the singlet-triplet decomposition, the Rashba spin-orbit coupling (SOC) boundary conditions can be written as follows, keeping only the terms of the first order in \hat{f} :

$$\begin{aligned} \partial_y f_{s,R} &= -mT_0T_1 \partial_z d_{x,L} \\ &\quad - 2 \left(\frac{T_0^2}{D} - 2 \frac{2}{3} \frac{T_1^2 p_F^2}{D} \right) (f_{s,L} - f_{s,R}), \end{aligned} \quad (39)$$

$$\begin{aligned} \partial_y d_{z,R} &= - \left(8d\alpha^2 - 2 \frac{T_0^2}{D} + 4 \frac{2}{3} \frac{T_1^2 p_F^2}{D} \right) d_{z,R} \\ &\quad - (2d_{z,L}) \left(\frac{T_0^2}{D} + 2 \frac{2}{3} \frac{T_1^2 p_F^2}{D} \right), \end{aligned} \quad (40)$$

$$\begin{aligned} \partial_y d_{x,R} &= -4 \partial_z f_{s,L} mT_0T_1 - \left(4 \frac{2}{3} \frac{T_1^2 p_F^2}{D} + 4d\alpha^2 - 2 \frac{T_0^2}{D} \right) d_{x,R} \\ &\quad - (2d_{x,L}) \frac{T_0^2}{D}, \end{aligned} \quad (41)$$

$$\partial_y d_{y,R} = - \left(4 \frac{2}{3} \frac{T_1^2 p_F^2}{D} + 4d\alpha^2 - 2 \frac{T_0^2}{D} \right) d_{y,R} - 2 \frac{T_0^2}{D} d_{y,L}. \quad (42)$$

From this, we see that there is a link between $f_{s,R}$ and $\partial_z d_{x,L}$ and the other way around between $d_{x,R}$ and $\partial_z f_{s,L}$. On the other hand, to first order, $d_{y,R}$ can only be induced by $d_{y,L}$, and $d_{z,R}$ can only be induced by $d_{z,L}$.

Furthermore, we can use the solution to the linearized Usadel equation in a normal metal:

$$\begin{aligned} f_s &= A_s e^{-ky} + B_s e^{ky}, \\ d_x &= A_x e^{-ky} + B_x e^{ky}, \end{aligned} \quad (43)$$

where $k = \sqrt{-2iE/D}$ and A_s, A_x, B_s , and B_x are constants that have to be determined using the boundary conditions. If we

assume that $l \rightarrow \infty$, the B factors have to be zero in order to avoid a diverging function.

A. Singlet current

We start by discussing the singlet charge current case. In this scenario, there are no triplet components present in (L). Thus there is no induced d_y or d_z on the right side of the interface. Furthermore, there is no d_x and thus no $\partial_y d_x$ on the left side. Assuming for simplicity $l \rightarrow \infty$, from Eqs. (39) and (41) we then see that

$$f_{s,R} \propto f_{s,L}, \quad (44)$$

$$d_{x,R} \propto \partial_z f_{s,L}, \quad (45)$$

since in this case $\partial_y f_{s,R} \propto f_{s,R}$ and $\partial_y d_{x,R} \propto d_{x,R}$. Note that the tilde-conjugated components have the same proportionality between the left and right sides. Thus it follows that

$$f_{s,L} \partial_z \tilde{f}_{s,L} - \tilde{f}_{s,L} \partial_z f_{s,L} \propto f_{s,R} \tilde{d}_{x,R} - \tilde{f}_{s,R} d_{x,R}. \quad (46)$$

From Eqs. (10) and (13) we see that the real part of the left side in the expression above is exactly what occurs in the expression for a singlet current in material (L), J_{f_s} . We also see that the real part of the right side in the expression is exactly what occurs in the induced magnetization expression $m_{x,R}$.

From the analytical expression, we conclude that there is a clear connection between induced magnetization and the singlet charge current. We note, however, that $f_{s,L} \partial_z \tilde{f}_{s,L} - \tilde{f}_{s,L} \partial_z f_{s,L}$ and $f_{s,R} \tilde{d}_{x,R} - \tilde{f}_{s,R} d_{x,R}$ might not have the same phase, such that the real part of these expressions might not be directly proportional.

B. Triplet charge current

Next, considering a triplet current, we see that the currents J_{d_y} and J_{d_z} , which contain varying d_y and d_z components in (L), do not induce a singlet in (R), at least to the first order in f . We can thus conclude that d_y and d_z induce no magnetization in (R). For the last type of triplet charge current, J_{d_x} , the same argumentation as for the singlet charge current applies. The difference is that in this case we have

$$d_{x,R} \propto d_{x,L}, \quad (47)$$

$$f_{s,R} \propto \partial_z d_{x,L}. \quad (48)$$

This gives

$$d_{x,L} \partial_z \tilde{d}_{x,L} - \tilde{d}_{x,L} \partial_z d_{x,L} \propto f_{s,R} \tilde{d}_{x,R} - \tilde{f}_{s,R} d_{x,R}. \quad (49)$$

Seemingly, J_{d_x} and J_{f_s} then induce the same magnetization.

A triplet charge current does, however, not have to be carried by a pure d_x , d_y , or d_z . In general, we can have an arbitrary \mathbf{d} vector carrying a pure charge current. Keeping to the situation where the triplet vector \mathbf{d} points in the xy plane, we would get a current carried partially by d_x and partially by d_y . In this case, the part carried by d_x induces a singlet component in (R), whereas the d_y part induces a d_y in (R) as well. By this argument, a magnetization in the y direction would also be induced. Thus we see that with a triplet charge current, magnetization can also be induced in more than one direction. This is contrary to the singlet charge current.

C. Spin current

We also briefly comment on how the induced magnetization changes when there is not only a charge supercurrent, but also a spin supercurrent flowing in (L). From Sec. III we see that there is no d_x component involved in the x -polarized current J_{s_x} . From this spin current, no singlet can be induced in (R), and thus also no magnetization. Both for the y -polarized spin current J_{s_y} and the z -polarized spin current J_{s_z} , a d_x component is involved. Since the d_y and d_z components are treated similarly by the spin-orbit coupled interface, we settle for only studying J_{s_z} . Presumably, J_{s_y} would induce a rotated, but similar magnetization.

The z -polarized spin current J_{s_z} is seen in Eq. (9) to be dependent on the imaginary part of the following expression:

$$d_{x,L} \partial_z \tilde{d}_{y,L} - d_{y,L} \partial_z \tilde{d}_{x,L} + \tilde{d}_{x,L} \partial_z d_{y,L} - \tilde{d}_{y,L} \partial_z d_{x,L}. \quad (50)$$

Notice that from the linearized spin-orbit coupled boundary conditions, it is found that

$$d_{y,L} \partial_z \tilde{d}_{x,L} \propto d_{y,R} \tilde{f}_{s,R}. \quad (51)$$

Notice also that the real part of the right side also occurs in the m_y expression. The relation here is much less direct than in the charge current and m_x case. In the expression for m_y the term and the tilde conjugation of the term are subtracted from each other, but in the J_{s_z} expression they are added together. Furthermore, m_y depends on the real part of the expression, whereas J_{s_z} depends on the imaginary part. It therefore follows that no clear connection exists between a pure spin current and an induced magnetization via the spin-orbit coupled interface.

D. Linearized spin-active boundary conditions

Before proceeding to the numerical study, we also look at the linearized spin-active boundary conditions in order to understand how the currents are created. These boundary conditions will only be used in interfaces where one side is a singlet superconductor. We consider below for concreteness the right interface and thus remove all triplets on the right side of the interface of the equations below. The linearized equations in the singlet-triplet decomposition notation read

$$\begin{aligned} \partial_z f_{s,L} = & -2\mathbf{m}^2(f_{s,L} + f_{s,R})G_1 + 2G_0 f_{s,R} - 2G_0 f_{s,L} \\ & - 2G_\phi(d_{x,L} m_x + d_{y,L} m_y + d_{z,L} m_z), \end{aligned} \quad (52)$$

$$\begin{aligned} \partial_z d_{x,L} = & (-\mathbf{m}^2 G_1 - 2G_0) d_{x,L} + (4id_{y,L} m_z - 4id_z m_y) G_{\text{MR}} \\ & - (2G_\phi) f_{s,L} m_x, \end{aligned} \quad (53)$$

$$\begin{aligned} \partial_z d_{y,L} = & (-2\mathbf{m}^2 G_1 - 2G_0) d_{y,L} + (4id_z m_x - 4im_z d_x) G_{\text{MR}} \\ & - (2G_\phi) f_{s,L} m_y, \end{aligned} \quad (54)$$

$$\begin{aligned} \partial_z d_{z,L} = & (-2\mathbf{m}^2 G_1 - 2G_0) d_{z,L} + (4id_x m_y - 4id_y m_x) G_{\text{MR}} \\ & - (2G_\phi) f_{s,L} m_z. \end{aligned} \quad (55)$$

For studying the triplet scenarios, material (L) will be a ferromagnet. Except for when we want to determine the effect of a current J_{d_z} , the exchange field will be oriented in the z direction, which induces a d_z component in (L). As mentioned, this d_z triplet will then be short ranged, and thus we focus

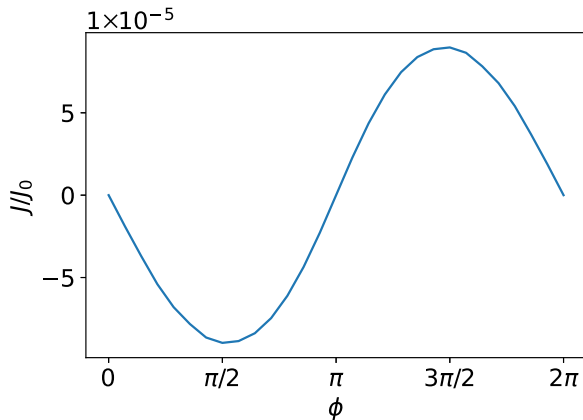


FIG. 5. The supercurrent induced in material (L) as a function of the phase difference between S1 and S2, ϕ . The boundary parameters used are $G_\phi = 0$, $P = 0$, $G_0 = 0.01/\xi_s$.

this discussion on the d_x and d_y components induced by the spin-active boundary.

The terms that create the d_x and d_y triplets are the G_ϕ and G_{MR} terms. If we only have the G_ϕ term, we see that the induced \mathbf{d} is parallel to the interface magnetization. If we, however, turn off G_ϕ but turn on G_{MR} (by letting $P \neq 0$), we see that \mathbf{d} is orthogonal to the interface magnetization, since d_z will already be present because of the exchange field in (L).

If we thus let the interface magnetizations be parallel to each other and only include one of the terms such that we have either $G_\phi = 0$ or $P = 0$, the behavior of the current closely resembles that of a conventional Josephson junction, except that it is only the triplet and not the singlet that is long ranged. Applying a phase difference between the BCS superconductors S1 and S2, it is reasonable to expect that in this case we can create a pure triplet charge current in (L). As we, in that case, are able to create only one long-ranged triplet component, we know there cannot be any spin current. When

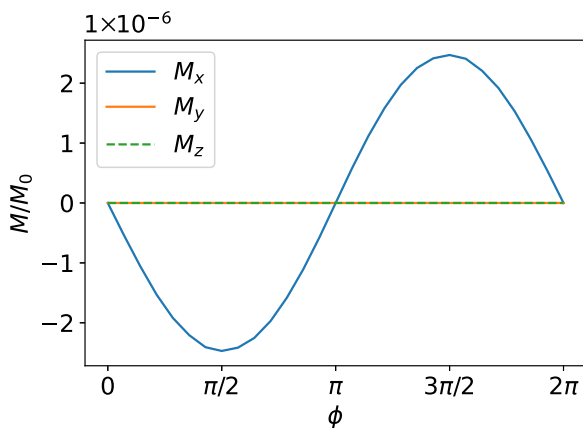


FIG. 6. The induced magnetization in (R), right next to the interface SOC interface at $y = 0$, in the presence of a supercurrent flow in region (L) due to a phase difference ϕ . The spin-active boundary parameters used are $G_\phi = 0$, $P = 0$, $G_0 = 0.01/\xi_s$, and the spin-orbit coupled boundary parameters used are $T_0^2/D = 0.2/\xi_s$, $\frac{2}{3}T_1^2 p_F^2/D = mT_0 T_1/\xi_s = d\alpha^2 = 0.1/\xi_s$.

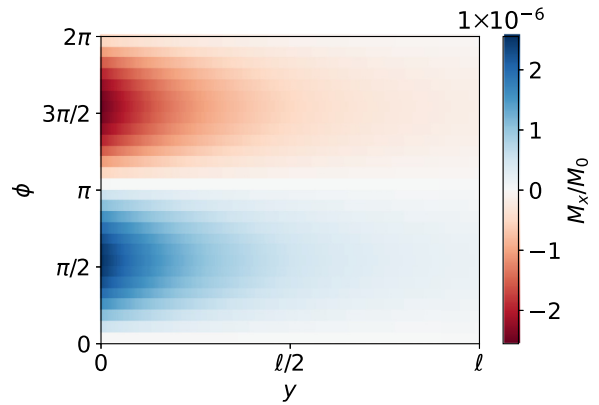


FIG. 7. The supercurrent-induced magnetization in (R) as a function of phase difference ϕ and position y in the zero-temperature case. The spin-active boundary parameters used are $G_\phi = 0$, $P = 0$, $G_0 = 0.01/\xi_s$, and the spin-orbit coupled boundary parameters used are $T_0^2/D = 0.2/\xi_s$, $\frac{2}{3}T_1^2 p_F^2/D = mT_0 T_1/\xi_s = d\alpha^2 = 0.1/\xi_s$.

both G_ϕ and G_{MR} are present, or $\theta \neq 0$, we see that both d_x and d_y will be created, and we can in general also find a spin supercurrent.

VII. NUMERICAL RESULTS

A. Singlet charge current

The proximity effect and magnetization induced by the singlet supercurrent are explored by removing the interface magnetizations and the exchange field in (L). We numerically determine the magnetization in the full-proximity-effect regime, using the nonlinear Riccati-parametrized equations, and compare it with the results expected from the analytical treatment. Furthermore, the role of the symmetry of the anomalous Green's function under the $\cdot \cdot \cdot$ operation is discussed. Finally, we discuss the spatial dependence of the magnetization induced in the normal metal (R) and also check the temperature dependency.

The current and magnetization as a function of ϕ are shown in Figs. 5 and 6. The magnetization shown in the Fig. 6 is evaluated at $y = 0$. As expected from the analytical study, no magnetization was induced in the y or z direction. Furthermore, it is seen from the figure that the induced m_x in (R) is proportional to the singlet current in (L). We remark that this is consistent with Ref. [29], whose authors found, from using an effective model for the Green's function in (L), that $m_x \propto J$. The effective model used in Ref. [29] has a disappearing derivative of f_s when $J = 0$ as it does not consider that the absolute value of f_s can be decaying. Inside a normal metal, however, we expect the Cooper pair wave function to decay away from the superconductor interfaces. Even when the current is zero, the singlet component can therefore still have a finite derivative. Therefore it is natural to ask whether the disappearance of the magnetization at $J = 0$ is caused by the spatial gradient of the $f_{s,L}$ and $d_{x,L}$ components vanishing at $\phi = 0, \pi$ or caused by the symmetry properties under the $\cdot \cdot \cdot$ operation of the triplet and singlet components. We have performed this analysis in Appendix C, and our conclusion is that the $\cdot \cdot \cdot$ -operation symmetry, which is influenced by

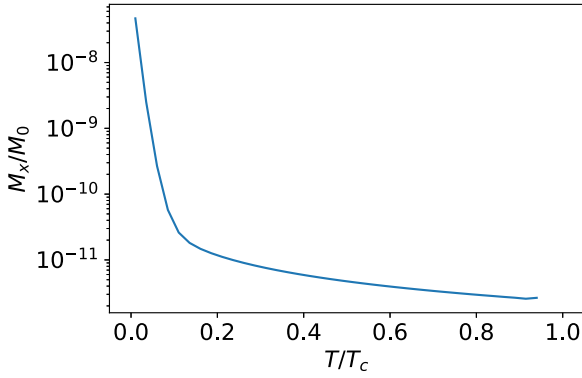


FIG. 8. The magnetization evaluated at $y = l$ as a function of temperature. We used $\phi = \pi/4$. The spin-active boundary parameters used are $G_\phi = 0$, $P = 0$, $G_0 = 0.01/\xi_s$, and the spin-orbit coupled boundary parameters used are $T_0^2/D = 0.2/\xi_s$, $\frac{2}{3}T_1^2 p_F^2/D = mT_0 T_1/\xi_s = d\alpha^2 = 0.1/\xi_s$.

whether or not a supercurrent flows, causes the magnetization to vanish at $\phi = 0, \pi$. Note that the absence of induced magnetization does not necessarily imply the absence of a triplet being induced. The supercurrent-induced magnetization decays monotonically in the (R) normal metal, as shown in Fig. 7.

Finally, we consider the temperature dependence of the supercurrent-induced magnetization. The quasiclassical magnetization from Eq. (13) has a factor $\tanh(\beta E/2)$ in the integrand. Varying the temperature changes how the contribution

$$\text{Re}(f_s(E)\tilde{d}_x(E) - \tilde{f}_s(E)d_x(E)) \quad (56)$$

is weighted with respect to energy. A relevant question to ask is therefore how the temperature affects the magnetization. The temperature dependence of the energy gap must be taken into account. We chose a standard interpolation formula which is valid for $T \in (0, T_c)$ [41]:

$$\Delta(T) = \Delta(0) \tanh\left(1.74\sqrt{\frac{T_c}{T} - 1}\right), \quad (57)$$

where T_c is the critical temperature. We also use the BCS relation between the zero-temperature gap and the critical temperature, $\frac{\Delta_0}{T_c} = 1.76$.

Figure 8 shows the magnetization evaluated at $y = l$ as a function of temperature. Although the integrand in general oscillates as a function of energy E , similarly to the spectral supercurrent, the total magnetization shows a monotonic decay with temperature.

B. Triplet charge current

In the following, the case with a pure triplet charge current is explored and compared with the singlet charge current case. To reduce the number of parameters to vary, this discussion only considers the zero-temperature case. We nevertheless expect a monotonic decay of the induced magnetization as the temperature approaches T_c .

To create a pure triplet charge current, as discussed in Sec. VI, the interface magnetizations have to be parallel.

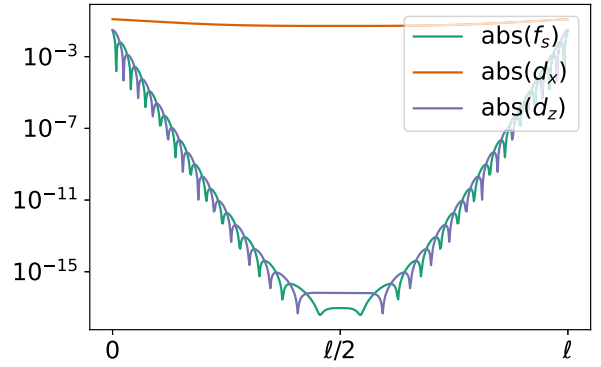


FIG. 9. The absolute value of the triplet components evaluated for $E/\Delta_0 = 0.14$. The figure shows that f_s and d_z are many orders of magnitude smaller than the long-ranged d_x component. The boundary parameters used are $P = 0$, $G_\phi = 3G_0$, $G_0 = 1/\xi_s$, $\alpha = 0$, $\theta = 0$.

Moreover, we also have to set either the polarization or the spin-mixing angles to zero. Otherwise, a spin supercurrent will also flow through the junction [42].

We first consider the $P = 0$ case, with a finite spin-mixing angle $G_\phi \neq 0$. This means only considering spin-independent transmission amplitudes from the proximate superconductor but with spin-dependent reflection terms.

We consider a situation where the f_s component is negligible compared with the triplets in (L). This is achieved via the exchange field profile discussed in Sec. V. Figure 9 shows that both f_s and d_z die out over a short range into the material (L) when $\mathbf{m}_1 = \mathbf{m}_2 = (m, 0, 0)$ and $\mathbf{h}(z) = (0, 0, h(z))$. The singlet and the d_z triplet oscillate rapidly and decay quickly [31,37]. In the middle region, d_z and f_s are many orders of magnitude smaller than d_x , and we conclude that the results from this section are pure triplet effects.

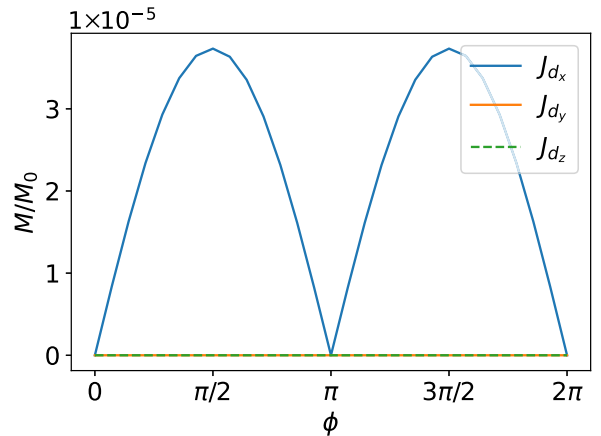


FIG. 10. The absolute value of the magnetization in material (R) induced by d_x -, d_y -, and d_z -carried charge current. It is seen that it is only the d_x -carried charge current that induces a magnetization. As seen, for certain triplet pair polarizations in any direction, a supercurrent (J_{d_y} and J_{d_z}) does not induce magnetization. The spin-orbit boundary parameters used are $T_0^2/D = 0.2/\xi_s$, $\frac{2}{3}T_1^2 p_F^2/D = mT_0 T_1/\xi_s = d\alpha^2 = 0.1/\xi_s$, and the spin-active boundary parameters used are $P = 0$, $G_\phi = 3G_0$, $G_0 = 1/\xi_s$, $\mathbf{m}_1 = \mathbf{m}_2 = (1, 0, 0), (0, 1, 0), (0, 0, 1)$ for the J_{d_x}, J_{d_y} , and J_{d_z} cases, respectively.

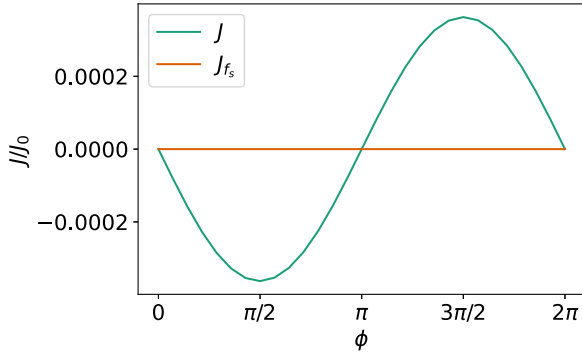


FIG. 11. Charge current as a function of ϕ in material (L). The green curve shows the total current, and the orange line shows the singlet current. It is clear that the singlet current is negligible compared with the triplet current. The magnitude of the triplet charge current is invariant when changing α . The boundary parameters used are $P = 0$, $G_\phi = 3G_0$, $G_0 = 1/\xi_s$, $\theta = 0$.

The triplet charge current can be divided into three components, J_{d_x} , J_{d_y} , and J_{d_z} , which from Sec. VI are expected to give different results. We explore all these currents here. A J_{d_x} current is created by using $\mathbf{m}_1 = \mathbf{m}_2 = (m, 0, 0)$ and $\mathbf{h} = (0, 0, h(z))$. In the same manner, a J_{d_y} current is created by using $\mathbf{m}_1 = \mathbf{m}_2 = (0, m, 0)$ and $\mathbf{h} = (0, 0, h(z))$, and a J_{d_z} current is created with $\mathbf{m}_1 = \mathbf{m}_2 = (0, 0, m)$ and $\mathbf{h} = (h(z), 0, 0)$. The absolute value of the induced magnetization in (R) is plotted for the three different triplet cases as a function of ϕ in Fig. 10. Consistent with the analysis in Sec. VI only the d_x -carried current induces a magnetization in (R), which confirms the analytical results. The induced magnetization can thereby be utilized to distinguish J_{d_x} from the other triplet currents. In other words, the induced spin signal is strongly dependent on the polarization of the triplet Cooper pair supercurrent.

However, a triplet current does not have to be carried by a pure d_x , d_y , or d_z , but could just as well be carried by any combination of \mathbf{d} -triplet components. Therefore rotation of

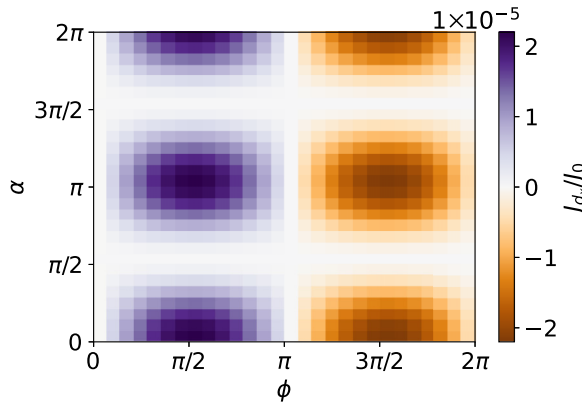


FIG. 12. The supercurrent carried by d_x triplet Cooper pairs, which induce a magnetization in (R) through the spin-orbit coupled interface, as both the phase difference ϕ and the interface angle in the xy plane, α , are varied. The boundary parameters used are $P = 0$, $G_\phi = 3G_0$, $G_0 = 1/\xi_s$, $\theta = 0$.

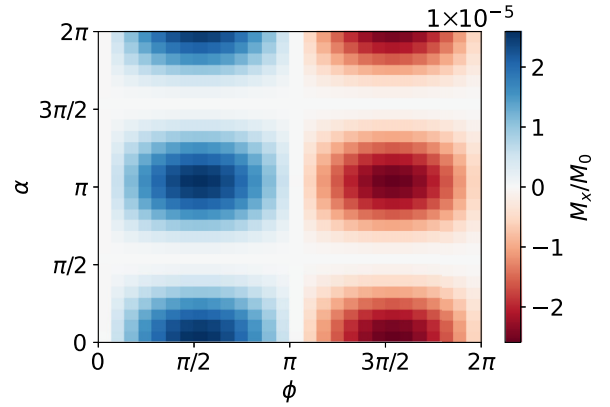


FIG. 13. Induced magnetization m_x in (L) in the triplet supercurrent case where $G_\phi \neq 0$, $P = 0$. The spin-orbit boundary parameters used are $T_0^2/D = 0.2/\xi_s$, $\frac{2}{3}T_1^2 p_F^2/D = mT_0T_1/\xi_s = d\alpha^2 = 0.1/\xi_s$, and the spin-active boundary parameters are $P = 0$, $G_\phi = 3G_0$, $G_0 = 1/\xi_s$, $\theta = 0$.

the interface magnetization in the xy plane is investigated. First, we consider the behavior of the charge current in material (L), shown in Fig. 11 as a function of the phase difference ϕ . The current shows a standard current-phase relation and is independent of the value of α . As seen in Sec. VI the G_ϕ term creates a \mathbf{d} vector proportional to the interface magnetization. At $\alpha = 0$ the interface magnetizations are $\mathbf{m}_1 = \mathbf{m}_2 = (m, 0, 0)$; so it is natural that the charge current then will be carried only by the d_x triplet. As α changes, the current will gradually be carried more and more by the d_y component, until it at $\alpha = \pi/2$ is carried only by the d_y components. Thus, as α is varied, the total current stays unchanged; however, J_{d_x} does change, as shown in Fig. 12.

The induced magnetization in material (R) in the triplet current case is plotted in Figs. 13 and 14. As discussed in Sec. VI, there exists a clear relation between J_{d_x} and $m_{x,R}$. Figure 13 confirms this relation as the induced m_x has the same form as J_{d_x} from Fig. 12.

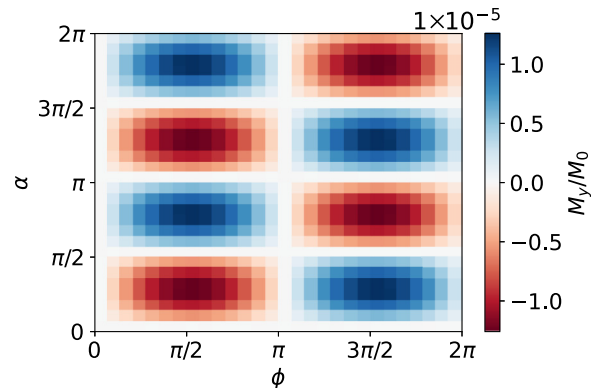


FIG. 14. Induced magnetization m_y in (L) in the triplet supercurrent case where $G_\phi \neq 0$, $P = 0$. The spin-orbit boundary parameters used are $T_0^2/D = 0.2/\xi_s$, $\frac{2}{3}T_1^2 p_F^2/D = mT_0T_1/\xi_s = d\alpha^2 = 0.1/\xi_s$, and the spin-active boundary parameters are $P = 0$, $G_\phi = 3G_0$, $G_0 = 1/\xi_s$, $\theta = 0$.

The magnetization plots also show differences from the singlet current case. First of all, the induced m_x varies with α . In the singlet case there is no interface magnetization; however, as varying α in the triplet case is the same as rotating the material (R) around material (L), it still makes sense to compare the α dependencies of the singlet case and the triplet case. What this means is that in the singlet case one would measure the same induced magnetization [in axes relative to (R)], no matter in what direction (R) was connected to (L). However, in the triplet case, the angle in which (R) is connected to (L) makes a difference.

Besides the α dependency in m_x , an additional new signature arises in the triplet case, namely a magnetization component in the y direction seen in Fig. 14. In the singlet current case, only m_x was induced, and thus the induced m_y contributes to making the triplet and singlet currents distinguishable. From the figure it is seen that m_y has a different α dependency than m_x . This can be explained by realizing that we expect $d_{x,L}$ and thus $\partial_z d_{x,L}$ to have a $\cos(\alpha)$ dependency. This would, according to the linearized spin-orbit coupled boundary conditions, give $d_{x,R}$ and $f_{s,R}$ both a $\cos(\alpha)$ dependency. Thus the induced magnetization m_x in (R), which is a product of $d_{x,R}$ and $f_{s,R}$, naturally acquires a $\cos^2(\alpha)$ dependency as in the figure. Furthermore, we should expect $d_{y,L}$ and thus also $d_{y,R}$ to have a $\sin(\alpha)$ dependency. The magnetization in the y direction, a product of $f_{s,R}$ and $d_{y,R}$, should therefore, consistent with the figure, have a $\sin(\alpha)\cos(\alpha)$ dependency.

If we compare the singlet current case with the triplet current at $\alpha = 0$, the induced magnetization in (R) looks the same. However, by either growing the normal metal on the (L) region at different crystallographic orientations, or alternatively growing two normal metals to (L), both through a spin-orbit coupling interface, but at different angles, the induced magnetization would change strongly in the triplet case. Similarly, as in the singlet case, we have checked that the disappearance of the magnetization at $\phi = 0$ and at $\phi = \pi$ can be explained by the symmetry properties under the $\cdot \cdot$ operation of the components. Thus we do not expect that a spatial gradient in the triplet correlations is sufficient to induce a magnetization: Only when a supercurrent is flowing, thus providing the triplet correlations with the correct $\cdot \cdot$ symmetry, is a magnetization induced.

In Fig. 15, we consider the dependence of the induced magnetization and the triplet supercurrent on the misalignment angle θ between the interfacial magnetic moments. This angle can be tuned experimentally by using different materials and/or thicknesses of the magnetic barriers. In such a case, the magnetization orientation of one barrier remains fixed upon applying an external magnetic field, whereas the magnetization of the (softer) barrier rotates with the field. We fix $\mathbf{m}_1 \parallel \mathbf{x}$ ($\alpha = 0$) and consider a superconducting phase difference $\phi = \pi/2$ which typically maximizes the supercurrent. The exchange field is fixed at $\mathbf{h} \parallel \mathbf{z}$, thus filtering out singlets f_s and the d_z triplets, as before. In the absence of misalignment ($\theta = 0$), the current is carried by d_x triplets, whereas no current is carried by d_y triplets. The ratio of the currents carried by these Cooper pairs changes upon varying θ , as seen in the lower row of Fig. 15. Both J_{d_x} and J_{d_y} are suppressed at $\theta = \pi/2$, in which case the magnetic texture

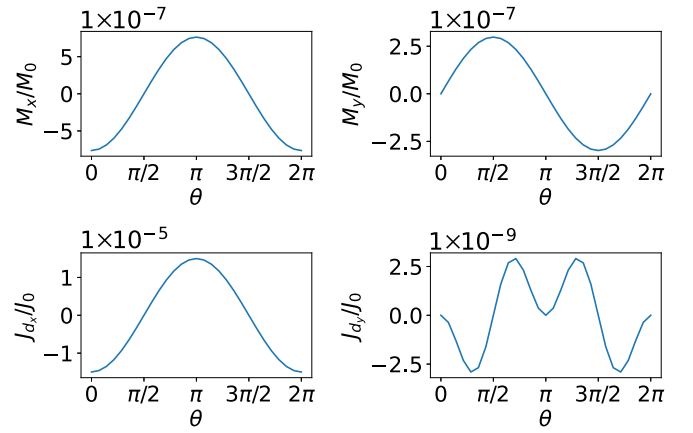


FIG. 15. Upper row: plots of the induced magnetization components. Lower row: the triplet supercurrent through the junction. The spin-orbit boundary parameters used are $T_0^2/D = 0.2/\xi_s$, $\frac{2}{3}T_1^2 p_F^2/D = mT_0 T_1/\xi_s = d\alpha^2 = 0.1/\xi_s$, and the spin-active boundary parameters are $P = 0$, $G_\phi = 3G_0$, $G_0 = 1/\xi_s$, with $\alpha = 0$ and varying θ .

of the system maximizes its spin chirality $(\mathbf{m}_1 \times \mathbf{m}_2) \cdot \mathbf{h}$. This can be understood as follows. Keeping \mathbf{m}_1 fixed in the x direction, there is always a d_x component induced at the $z = 0$ interface. Keeping the phase difference fixed to $\phi = \pi/2$, the amount of supercurrent J_{d_x} then depends on the induced d_x on the $x = l$ interface. The d_x on this side will be proportional to $m_{2,x} \propto \cos(\theta)$ since it is primarily induced from singlet conversion at the $x = l$ interface. Figure 15 shows that J_{d_x} has precisely this θ dependency and so vanishes at $\theta = \pi/2$. For the d_y , on the other hand, there is no directly induced d_y from singlet conversion at the $z = 0$ interface, and thus one cannot immediately read out the phase or tilde-conjugation properties of d_y from the linearized equations. Since d_y is only directly induced at the $z = l$ interface, it is nevertheless reasonable to expect that J_{d_y} is smaller than J_{d_x} , which is consistent with Fig. 15.

Consider now the resulting induced spin magnetization in the normal metal and its dependence on θ , shown in the upper row of Fig. 15. The m_x component follows the current carried by d_x triplets, as in the previous cases considered in this paper. The m_y component, however, does not follow the d_y triplets. In fact, the m_y component is maximal at $\theta = \pi/2$, where $J_{d_y} = 0$. This can be understood by considering the tilde-conjugation properties of the individual d_x and d_y components. The argument is most easily presented by considering the phase of S1 to be 0 and the phase of S2 to be ϕ , although the physics naturally only depends on the actual value of the phase difference. At $\phi = \pi/2$ the singlet superconductors S1 and S2 behave oppositely under tilde conjugation, $\tilde{f}_{s,1} = -f_{s,1}$, $\tilde{f}_{s,2} = -f_{s,2}e^{2i\phi} = +f_{s,2}$. Thus we should also expect d_x and d_y to have opposite tilde-conjugation properties at $\theta = \pi/2$ since they are induced at different interfaces. We see that there is no J_{d_x} at $\theta = \pi/2$, which means that $\partial_z d_x$ and d_x have the same tilde-conjugation property, and thus by the SOC boundary conditions, $f_{s,R}$ will also inherit this tilde-conjugation property. Furthermore, since $d_{y,R}$ inherits the tilde-conjugation property of $d_{y,L}$, we have

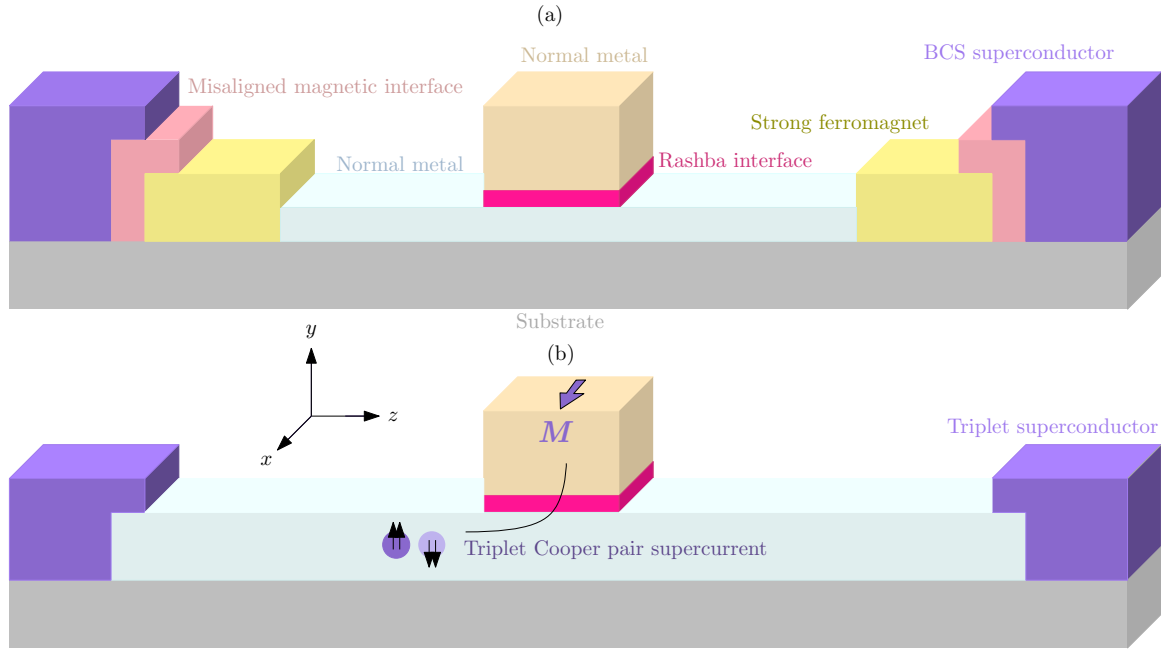


FIG. 16. Two possible experimental realizations of the proposed system. In (a), thin magnetic insulators with a magnetization in the xy plane couple BCS superconductors to a strong ferromagnet which is polarized in the z direction. The strong ferromagnet filters out all superconducting correlations except equal-spin Cooper pairs along the magnetization direction. Adjusting the magnetization of the magnetic interfaces allows one to vary the spin polarization of the triplet Cooper pairs carrying a supercurrent in the system. A simpler setup is shown in (b), where one uses intrinsic triplet superconductors. By growing these materials along different crystallographic axes relative to the normal metal in the middle, the polarization of the triplet pairs, quantified by the \mathbf{d} vector, is varied. The drawback of the setup in (b) is that intrinsic p -wave triplet superconductivity is rare and is only well established in uranium-based compounds.

$d_{y,R}$ and $f_{s,R}$ with opposite tilde-conjugation properties, which leads to an induced m_y as seen in Fig. 15.

Finally, to check the robustness of the results, another parameter set was also investigated. The interface magnetizations are kept parallel; however, the polarization is turned on, adding the magnetoresistive term and the G_1 term. Instead the spin mixing is turned off, $G_\phi = 0$. From Sec. VI we see that the G_{MR} term creates a triplet \mathbf{d} orthogonal to the interface magnetization and to \mathbf{h} . In this case, a $\pi/2$ shift in α arises compared with the $P = 0$ situation because of the induced triplet being orthogonal to the interface magnetization instead of parallel. Other than that, the form of the magnetization is similar, and the conclusions from the $P = 0$ case hold.

VIII. CONCLUSION

In summary, we predict an experimental signature of current-carrying triplet Cooper pairs in the form of an induced spin signal. We show that a supercurrent carried only by triplet Cooper pairs induces a nonlocal magnetization that is controlled by the polarization direction of the triplet Cooper pairs. The dependence of the nonlocal magnetization on the polarization direction of the triplet pairs can be experimentally tested *in situ*. Specifically, the component of the \mathbf{d} vector carrying the supercurrent is determined by the magnetizations in Fig. 16. This provides a measurement protocol to directly use the spin polarization of the triplet Cooper pairs in supercurrents to transfer spin information in a dissipationless manner.

ACKNOWLEDGMENTS

This work was supported by the Research Council of Norway through Grant No. 323766 and its Centres of Excellence funding scheme, Grant No. 262633 “QuSpin.” Support from Sigma2 - the National Infrastructure for High Performance Computing and Data Storage in Norway, Project No. NN9577K, is acknowledged.

APPENDIX A: RICCATI PARAMETRIZATION OF THE SOC BOUNDARY CONDITIONS

We now derive the Riccati parametrization of spin-orbit coupling boundary conditions given in Eq. (4). These boundary conditions take into account charge-spin conversion at the interface [29]. The starting point is to perform the same operation on the right-hand side as we did on the left-hand side in Eq. (28). The first term is simply the Kuprianov-Lukichev boundary term [36]. The rest of the terms we go through one by one. For concreteness, the derivation below is done for a boundary condition which has $g_R \partial_y g_R$ on the left-hand side of the boundary condition.

The first term is $-\frac{2}{3} T_1^2 p_F^2 [\hat{g}_R, \hat{\tau}_\parallel \hat{g}_L \hat{\tau}_\parallel]$, for which we define the matrix

$$\begin{aligned} \hat{U}^{(1)} &= \hat{\tau}_\parallel \hat{g}_L \hat{\tau}_\parallel \\ &= \begin{pmatrix} \tau_x g_L \tau_x & -\tau_x f_L \tau_x^* \\ \tau_x^* \tilde{f}_L \tau_x & -\tau_x^* \tilde{g}_L \tau_x^* \end{pmatrix} + \begin{pmatrix} \tau_z g_L \tau_z & -\tau_z f_L \tau_z^* \\ \tau_z^* \tilde{f}_L \tau_z & -\tau_z^* \tilde{g}_L \tau_z^* \end{pmatrix}. \end{aligned} \quad (\text{A1})$$

Thus the contribution from this term will, according to Eq. (35), be

$$\begin{aligned} & \frac{1}{2}N_R^{-1}([\hat{g}_R, \hat{\tau}_{\parallel}\hat{g}_L\hat{\tau}_{\parallel}]^{1,2} - [\hat{g}_R, \hat{\tau}_{\parallel}\hat{g}_L\hat{\tau}_{\parallel}]^{1,1})\gamma_R \\ &= [-(\tau_x g_L \tau_x + \tau_z g_L \tau_z)\gamma_R - \tau_x f_L \tau_x^* - \tau_z f_L \tau_z^* \\ & \quad - \gamma_R(\tau_x^* \tilde{f}_L \tau_x + \tau_z^* \tilde{f}_L \tau_z)\gamma_R + \gamma_R(-\tau_x^* \tilde{g}_L \tau_x^* - \tau_z^* \tilde{g}_L \tau_z^*)], \end{aligned} \quad (\text{A2})$$

and inserting $f = 2N\gamma$ and $g = (2N - 1)$, we get

$$\begin{aligned} & -\tau_x N_L \tau_x \gamma_R + \gamma_R - \tau_x N_L \gamma_L \tau_x^* - \gamma_R \tau_x^* \tilde{N}_L \tilde{\gamma}_L \tau_x \gamma_R - \gamma_R \tau_x^* \tilde{N}_L \tau_x^* \\ & -\tau_z N_L \tau_z \gamma_R + \gamma_R - \tau_z N_L \gamma_L \tau_z^* - \gamma_R \tau_z^* \tilde{N}_L \tilde{\gamma}_L \tau_z \gamma_R - \gamma_R \tau_z^* \tilde{N}_L \tau_z^*. \end{aligned} \quad (\text{A3})$$

From the second term we define

$$\begin{aligned} \hat{U}^{(2)} &= \{\hat{\tau}_{\parallel,x}, \hat{g}_L \partial_y \hat{g}_L\} \\ &= \begin{pmatrix} \tau_x [g_L g'_L - f_L \tilde{f}'_L] & \tau_x [g_L f'_L - f_L \tilde{g}'_L] \\ -\tau_x^* [\tilde{f}_L \tilde{g}'_L + \tilde{g}_L \tilde{f}'_L] & -\tau_x [-\tilde{f}_L f'_L + \tilde{g}_L \tilde{g}'_L] \end{pmatrix} \\ & \quad + \begin{pmatrix} [g_L g'_L - f_L \tilde{f}'_L] \tau_x & -[g_L f'_L - f_L \tilde{g}'_L] \tau_x^* \\ [\tilde{f}_L \tilde{g}'_L + \tilde{g}_L \tilde{f}'_L] \tau_x & [-\tilde{f}_L f'_L + \tilde{g}_L \tilde{g}'_L] \tau_x^* \end{pmatrix}, \end{aligned} \quad (\text{A4})$$

which gives us the contribution to the right-hand side

$$\begin{aligned} & [-(\tau_x [g_L g'_L - f_L \tilde{f}'_L] + [g_L g'_L - f_L \tilde{f}'_L] \tau_x) \gamma_R \\ & \quad + \tau_x [g_L f'_L - f_L \tilde{g}'_L] - [g_L f'_L - f_L \tilde{g}'_L] \tau_x^* \\ & \quad - \gamma_R(-\tau_x^* [\tilde{f}_L \tilde{g}'_L + \tilde{g}_L \tilde{f}'_L] + [\tilde{f}_L \tilde{g}'_L + \tilde{g}_L \tilde{f}'_L] \tau_x) \gamma_R \\ & \quad + \gamma_R(-\tau_x [-\tilde{f}_L f'_L + \tilde{g}_L \tilde{g}'_L] - [-\tilde{f}_L f'_L + \tilde{g}_L \tilde{g}'_L] \tau_x^*)]. \end{aligned} \quad (\text{A5})$$

Using Eqs. (21) and (22), we see that we can write the following:

$$\begin{aligned} [g_L g'_L - f_L \tilde{f}'_L] &= N_L [\gamma'_L \tilde{\gamma}_L - \gamma_L \tilde{\gamma}'_L] N_L, \\ [g_L f'_L - f_L \tilde{g}'_L] &= N_L [\gamma'_L - \gamma_L \tilde{\gamma}'_L \gamma_L] \tilde{N}_L. \end{aligned} \quad (\text{A6})$$

Thus the contribution to the right-hand side of the Riccati-parametrized boundary conditions can be written as

$$\begin{aligned} & \tau_x 2N_L [\gamma'_L - \gamma_L \tilde{\gamma}'_L \gamma_L] \tilde{N}_L - 2N_L [\gamma'_L - \gamma_L \tilde{\gamma}'_L \gamma_L] \tilde{N}_L \tau_x^* \\ & \quad - \gamma_R \tau_x^* 2\tilde{N}_L [\tilde{\gamma}'_L \gamma_L - \tilde{\gamma}_L \gamma'_L] \tilde{N}_L - \gamma_R 2\tilde{N}_L [\tilde{\gamma}'_L \gamma_L - \tilde{\gamma}_L \gamma'_L] \tilde{N}_L \tau_x^* \\ & \quad - \tau_x 2N_L [\gamma'_L \tilde{\gamma}_L - \gamma_L \tilde{\gamma}'_L] N_L \gamma_R - 2N_L [\gamma'_L \tilde{\gamma}_L - \gamma_L \tilde{\gamma}'_L] N_L \tau_x \gamma_R \\ & \quad + \gamma_R \tau_x^* 2\tilde{N}_L [\tilde{\gamma}'_L - \tilde{\gamma}_L \gamma'_L \tilde{\gamma}_L] N_L \gamma_R - \gamma_R 2\tilde{N}_L [\tilde{\gamma}'_L \\ & \quad - \tilde{\gamma}_L \gamma'_L \tilde{\gamma}_L] N_L \tau_x \gamma_R. \end{aligned} \quad (\text{A7})$$

The fourth term and fifth term in Eq. (4) cannot be written as $[g_R, \hat{U}]$; so we have to treat them differently. The two terms do, however, have the same form as each other. Therefore we only have to perform the calculation once by performing the parametrization procedure on

$$[\hat{\rho}_i, \hat{g}_R \hat{\rho}_i \hat{g}_R]. \quad (\text{A8})$$

We write out

$$g_R \hat{\rho}_i g_R = \begin{pmatrix} g_R \tau_i g_R + f_R \tau_i^* \tilde{f}_R & g_R \tau_i f_R + f_R \tau_i^* \tilde{g}_R \\ -\tilde{f}_R \tau_i g_R - \tilde{g}_R \tau_i^* \tilde{f}_R & -\tilde{f}_R \tau_i f_R - \tilde{g}_R \tau_i^* \tilde{g}_R \end{pmatrix}. \quad (\text{A9})$$

The upper left component of the whole expression then reads

$$\begin{aligned} [\hat{\rho}_i, \hat{g}_R \hat{\rho}_i \hat{g}_R]_{(11)} &= \tau_i g_R \tau_i g_R + \tau_i f_R \tau_i^* \tilde{f}_R - g_R \tau_i g_R \tau_i \\ & \quad - f_R \tau_i^* \tilde{f}_R \tau_i, \end{aligned} \quad (\text{A10})$$

and the upper right part reads

$$\begin{aligned} [\hat{\rho}_i, \hat{g}_R \hat{\rho}_i \hat{g}_R]_{(12)} &= \tau_i g_R \tau_i f_R + \tau_i f_R \tau_i^* \tilde{g}_R + g_R \tau_i f_R \tau_i^* \\ & \quad + f_R \tau_i^* \tilde{g}_R \tau_i^*. \end{aligned} \quad (\text{A11})$$

We write g and f in terms of the Riccati-parametrized expressions and get that the contribution from these terms to the right-hand side $\frac{1}{2}N_L^{-1}((1, 2) - (1, 1)) \frac{1}{2}N_R^{-1}((1, 2) - (1, 1))$ is

$$\begin{aligned} & \frac{1}{2}N_R^{-1}[\tau_i(2N_R - 1)\tau_i 2N_R \gamma_R + \tau_i 2N_R \gamma_R \tau_i^*(2\tilde{N}_R - 1) + (2N_R - 1)\tau_i 2N_R \gamma_R \tau_i^* \\ & \quad + 2N_R \gamma_R \tau_i^*(2\tilde{N}_R - 1)\tau_i^* - [\tau_i(2N_R - 1)\tau_i(2N_R - 1) + \tau_i 2N_R \gamma_R \tau_i^* 2\tilde{N}_R \tilde{\gamma}_R \\ & \quad - (2N_R - 1)\tau_i(2N_R - 1)\tau_i - 2N_R \gamma_R \tau_i^* 2\tilde{N}_R \tilde{\gamma}_R] \gamma_R] \\ & = -2\gamma_R + 2\tau_i N_R \gamma_R \tau_i^* + 2\gamma_R \tau_i^* \tilde{N}_R \tau_i^* + 2\tau_i N_R \tau_i \gamma_R + 2\gamma_R \tau_i^* \tilde{N}_R \tilde{\gamma}_R \tau_i \gamma_R. \end{aligned} \quad (\text{A12})$$

Putting all of the terms together, we get

$$\begin{aligned} \partial_y \gamma_R &= 2 \frac{T_0^2}{D} (1 - \gamma_R \tilde{\gamma}_L) N_L (\gamma_R - \gamma_L) \\ & \quad - 2 \frac{T_1^2 p_F^2}{3 D} (-\tau_x N_L \tau_x \gamma_R + \gamma_R - \tau_x N_L \gamma_L \tau_x^* - \gamma_R \tau_x^* \tilde{N}_L \tilde{\gamma}_L \tau_x \gamma_R - \gamma_R \tau_x^* \tilde{N}_L \tau_x^* \\ & \quad - \tau_z N_L \tau_z \gamma_R + \gamma_R - \tau_z N_L \gamma_L \tau_z^* - \gamma_R \tau_z^* \tilde{N}_L \tilde{\gamma}_L \tau_z \gamma_R - \gamma_R \tau_z^* \tilde{N}_L \tau_z^*) \\ & \quad - m T_1 T_0 (+\tau_x 2N_L [\gamma'_L - \gamma_L \tilde{\gamma}'_L \gamma_L] \tilde{N}_L - 2N_L [\gamma'_L - \gamma_L \tilde{\gamma}'_L \gamma_L] \tilde{N}_L \tau_x^* \\ & \quad - \gamma_R \tau_x^* 2\tilde{N}_L [\tilde{\gamma}'_L \gamma_L - \tilde{\gamma}_L \gamma'_L] \tilde{N}_L - \gamma_R 2\tilde{N}_L [\tilde{\gamma}'_L \gamma_L - \tilde{\gamma}_L \gamma'_L] \tilde{N}_L \tau_x^* \end{aligned}$$

$$\begin{aligned}
& -\tau_x 2N_L[\gamma'_L \tilde{\gamma}_L - \gamma_L \tilde{\gamma}'_L] N_L \gamma_R - 2N_L[\gamma'_L \tilde{\gamma}_L - \gamma_L \tilde{\gamma}'_L] N_L \tau_x \gamma_R \\
& + \gamma_R \tau_x^* 2\tilde{N}_L[\tilde{\gamma}'_L - \tilde{\gamma}_L \gamma'_L \tilde{\gamma}_L] N_L \gamma_R - \gamma_R 2\tilde{N}_L[\tilde{\gamma}'_L - \tilde{\gamma}_L \gamma'_L \tilde{\gamma}_L] N_L \tau_x \gamma_R \\
& + d\alpha^2(-2\gamma_R + 2\tau_x N_R \gamma_R \tau_x^* + 2\gamma_R \tau_x^* \tilde{N}_R \tau_x^* + 2\tau_x N_R \tau_x \gamma_R + 2\gamma_R \tau_x^* \tilde{N}_R \tilde{\gamma}_R \tau_x \gamma_R) \\
& + d\alpha^2(-2\gamma_R + 2\tau_z N_R \gamma_R \tau_z^* + 2\gamma_R \tau_z^* \tilde{N}_R \tau_z^* + 2\tau_z N_R \tau_z \gamma_R + 2\gamma_R \tau_z^* \tilde{N}_R \tilde{\gamma}_R \tau_z \gamma_R). \tag{A13}
\end{aligned}$$

APPENDIX B: RICCATI PARAMETRIZATION OF THE SPIN-ACTIVE BOUNDARY CONDITIONS

We now find the Riccati-parametrized boundary conditions for the spin-active interfaces given in Eq. (2). All the terms on this boundary condition are in the same form as in Eq. (26). Just as for the spin-orbit coupling boundary conditions, the first term is simply the Kuprianov-Lukichev term; the rest we go through one term at a time starting with the G_1 term. Here we define

$$U_1 = \hat{m} \hat{g}_R \hat{m} = \begin{pmatrix} \mathbf{m} \cdot \boldsymbol{\tau} g_R \mathbf{m} \cdot \boldsymbol{\tau} & \mathbf{m} \cdot \boldsymbol{\tau} f_R \mathbf{m} \cdot \boldsymbol{\tau}^* \\ -\mathbf{m} \cdot \boldsymbol{\tau}^* \tilde{f}_R \mathbf{m} \cdot \boldsymbol{\tau} & -\mathbf{m} \cdot \boldsymbol{\tau}^* \tilde{g}_R \mathbf{m} \cdot \boldsymbol{\tau}^* \end{pmatrix}, \tag{B1}$$

which gives the contribution to the right-hand side

$$-\mathbf{m} \cdot \boldsymbol{\tau} g_R \mathbf{m} \boldsymbol{\tau} \gamma_L + \mathbf{m} \boldsymbol{\tau} f_R \mathbf{m} \boldsymbol{\tau}^* + \gamma_L \mathbf{m} \boldsymbol{\tau}^* \tilde{f}_R \mathbf{m} \boldsymbol{\tau} \gamma_L - \gamma_L \mathbf{m} \boldsymbol{\tau}^* \tilde{g}_R \mathbf{m} \boldsymbol{\tau}^*. \tag{B2}$$

For the second term we define the U matrix

$$U_{MR} = \{\hat{g}_R, \hat{m}\} = \begin{pmatrix} g_R \mathbf{m} \cdot \boldsymbol{\tau} + \mathbf{m} \cdot \boldsymbol{\tau} g_R & f_R \mathbf{m} \cdot \boldsymbol{\tau}^* + \mathbf{m} \cdot \boldsymbol{\tau} f_R \\ -\tilde{f}_R \mathbf{m} \cdot \boldsymbol{\tau} - \mathbf{m} \cdot \boldsymbol{\tau}^* \tilde{f}_R & -\tilde{g}_R \mathbf{m} \cdot \boldsymbol{\tau}^* - \mathbf{m} \cdot \boldsymbol{\tau}^* \tilde{g}_R \end{pmatrix}, \tag{B3}$$

which gives the contribution to the right-hand side

$$\begin{aligned}
& -(g_R \mathbf{m} \cdot \boldsymbol{\tau} + \mathbf{m} \cdot \boldsymbol{\tau} g_R) \gamma_L + f_R \mathbf{m} \cdot \boldsymbol{\tau}^* + \mathbf{m} \cdot \boldsymbol{\tau} f_R \\
& - \gamma_L (-\tilde{f}_R \mathbf{m} \cdot \boldsymbol{\tau} - \mathbf{m} \cdot \boldsymbol{\tau}^* \tilde{f}_R) \gamma_L \\
& + \gamma_L (-\tilde{g}_R \mathbf{m} \cdot \boldsymbol{\tau}^* - \mathbf{m} \cdot \boldsymbol{\tau}^* \tilde{g}_R). \tag{B4}
\end{aligned}$$

For the third term the U matrix is simply $U_\phi = \hat{m}$, which gives the contribution

$$-\mathbf{m} \cdot \boldsymbol{\tau} \gamma_L + \gamma_L \mathbf{m} \cdot \boldsymbol{\tau}^*. \tag{B5}$$

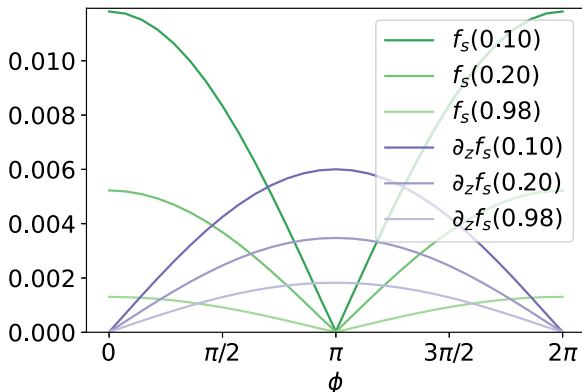


FIG. 17. The absolute value of the singlet component $f_s(E/\Delta_0)$ and its derivative in material (L) at $z_0 = l/2$.

The total Riccati-parametrized spin-active boundary conditions thus read

$$\begin{aligned}
\partial_z \gamma_L &= G_0(1 - \gamma_L \tilde{\gamma}_R) N_R (\gamma_R - \gamma_L) \\
&+ G_1(\mathbf{m} \cdot \boldsymbol{\tau} N_R \gamma_R \mathbf{m} \cdot \boldsymbol{\tau}^* - \gamma_L \mathbf{m} \cdot \boldsymbol{\tau}^* \tilde{N}_R \mathbf{m} \cdot \boldsymbol{\tau}^* + m^2 \gamma_L \\
&- \mathbf{m} \cdot \boldsymbol{\tau} N_R \mathbf{m} \cdot \boldsymbol{\tau} \gamma_L + \gamma_L \mathbf{m} \cdot \boldsymbol{\tau}^* \tilde{N}_R \tilde{\gamma}_R \mathbf{m} \cdot \boldsymbol{\tau} \gamma_L) \\
&+ G_{MR}(N_R \gamma_R \mathbf{m} \cdot \boldsymbol{\tau}^* + \mathbf{m} \cdot \boldsymbol{\tau} N_R \gamma_R \\
&- \gamma_L[\tilde{N}_R \mathbf{m} \cdot \boldsymbol{\tau}^* + \mathbf{m} \cdot \boldsymbol{\tau}^* \tilde{N}_R - \mathbf{m} \cdot \boldsymbol{\tau}^*] \\
&- [N_R \mathbf{m} \cdot \boldsymbol{\tau} - \mathbf{m} \cdot \boldsymbol{\tau} + \mathbf{m} \cdot \boldsymbol{\tau} N_R] \gamma_L \\
&+ \gamma_L[\tilde{N}_R \tilde{\gamma}_R \mathbf{m} \cdot \boldsymbol{\tau} + \mathbf{m} \cdot \boldsymbol{\tau}^* \tilde{N}_R \tilde{\gamma}_R] \gamma_L) \\
&- iG_\phi(-\mathbf{m} \cdot \boldsymbol{\tau} \gamma_L + \gamma_L \mathbf{m} \cdot \boldsymbol{\tau}^*). \tag{B6}
\end{aligned}$$

APPENDIX C: ANALYSIS OF THE SYMMETRY OF THE ANOMALOUS GREEN'S FUNCTION UNDER THE $\cdot \tilde{\cdot}$ OPERATION

We here analyze whether the disappearance of the magnetization at $J = 0$ is caused by the spatial gradient of the $f_{s,R}$ and $d_{x,R}$ components at $\phi = 0, \pi$ or by the symmetry properties under the $\cdot \tilde{\cdot}$ operation of the triplet and singlet components. To investigate this, consider Figs. 17 and 18. The first situation explored is when material (R) is connected to the middle of material (L), $z_0 = l/2$. It is seen from the figures that in this case the singlet component, $f_{s,L}$, is zero at $\phi = \pi$ while the derivative, $\partial_z f_{s,L}$, is zero at $\phi = 0$. The figures show that this also causes $d_{x,R}$ to vanish at $\phi = 0$ and $f_{s,R}$ at $\phi = \pi$. Thus a finite derivative of f_s is not sufficient to induce a magnetization in (R).

To check whether it is the symmetry of the anomalous Green's function under the $\cdot \tilde{\cdot}$ operation that dictates when

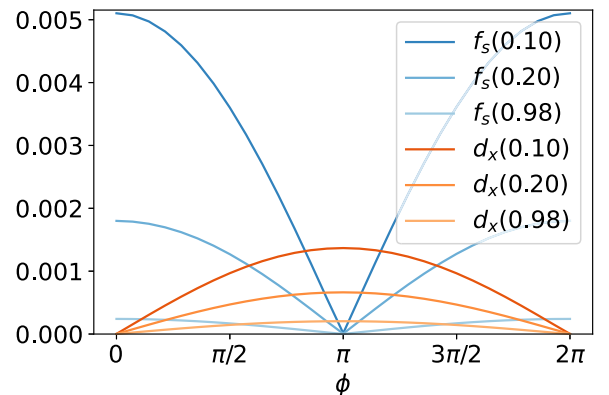


FIG. 18. The absolute value of the components $f_s(E/\Delta_0)$ and $d_x(E/\Delta_0)$ in material (R) as a function of ϕ for different energies, E/Δ_0 , at $z_0 = l/2$.

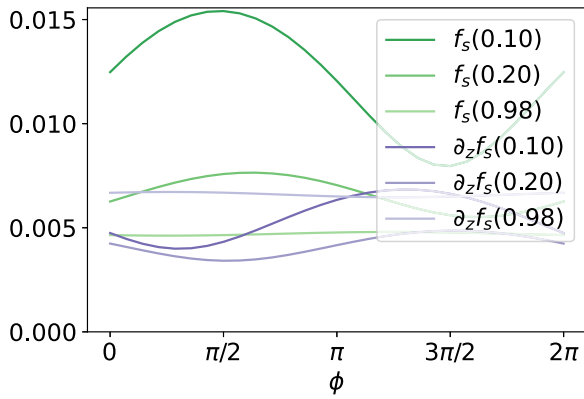


FIG. 19. The absolute value of the singlet component $f_s(E/\Delta_0)$ and its derivative in material (L) at $z_0 = l/4$.

a finite magnetization occurs, we considered a different situation where $z_0 = l/4$ so that the material (R) is no longer connected to the middle of (L). The result is shown in Figs. 19 and 20. It is here seen that neither $f_{s,L}$ nor $\partial_z f_{s,L}$ vanishes at any ϕ . Therefore also $d_{x,R}$ and $f_{s,R}$ are finite at every ϕ . It

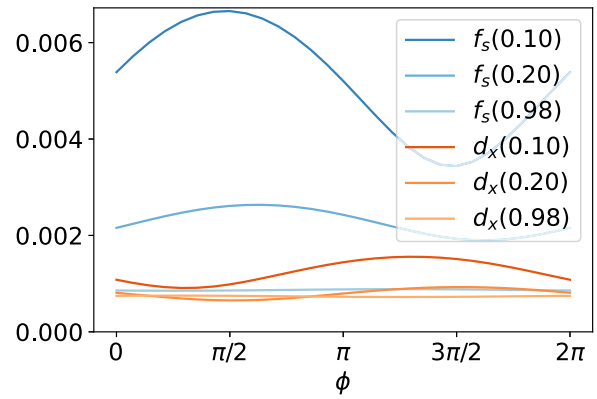


FIG. 20. The absolute value of the components $f_s(E/\Delta_0)$ and $d_x(E/\Delta_0)$ in material (R) as a function of ϕ for different energies, E/Δ_0 , at $z_0 = l/4$.

was checked that the magnetization looks exactly like that in Fig. 6, also for $z_0 = l/4$. Thus we can conclude that it is the π -operation symmetry, which is influenced by whether or not a supercurrent flows, that causes the magnetization to vanish at $\phi = 0, \pi$.

-
- [1] M. Eschrig, A. Cottet, W. Belzig, and J. Linder, *New J. Phys.* **17**, 083037 (2015).
- [2] J. Linder and J. W. A. Robinson, *Nat. Phys.* **11**, 307 (2015).
- [3] C. Bell, S. Milikisyants, M. Huber, and J. Aarts, *Phys. Rev. Lett.* **100**, 047002 (2008).
- [4] K. R. Jeon, C. Ciccarelli, A. J. Ferguson, H. Kurebayashi, L. F. Cohen, X. Montiel, M. Eschrig, J. W. Robinson, and M. G. Blamire, *Nat. Mater.* **17**, 499 (2018).
- [5] K.-R. Jeon, C. Ciccarelli, H. Kurebayashi, L. F. Cohen, S. Komori, J. W. A. Robinson, and M. G. Blamire, *Phys. Rev. B* **99**, 144503 (2019).
- [6] Y. Yao, R. Cai, T. Yu, Y. Ma, W. Xing, Y. Ji, X.-C. Xie, S.-H. Yang, and W. Han, *Sci. Adv.* **7**, eabh3686 (2021).
- [7] M. Müller, L. Liensberger, L. Flacke, H. Huebl, A. Kamra, W. Belzig, R. Gross, M. Weiler, and M. Althammer, *Phys. Rev. Lett.* **126**, 087201 (2021).
- [8] S. J. Carreira, D. Sanchez-Manzano, M.-W. Yoo, K. Seurre, V. Rouco, A. Sander, J. Santamaría, A. Anane, and J. E. Villegas, *Phys. Rev. B* **104**, 144428 (2021).
- [9] R. S. Keizer, S. T. B. Goennenwein, T. M. Klapwijk, G. Miao, and A. Gupta, *Nature (London)* **439**, 825 (2006).
- [10] J. W. A. Robinson, J. D. S. Witt, and M. G. Blamire, *Science* **329**, 59 (2010).
- [11] T. S. Khaire, M. A. Khasawneh, W. P. Pratt, and N. O. Birge, *Phys. Rev. Lett.* **104**, 137002 (2010).
- [12] M. Houzet, *Phys. Rev. Lett.* **101**, 057009 (2008).
- [13] T. Yokoyama and Y. Tserkovnyak, *Phys. Rev. B* **80**, 104416 (2009).
- [14] T. Kato, Y. Ohnuma, M. Matsuo, J. Rech, T. Jonckheere, and T. Martin, *Phys. Rev. B* **99**, 144411 (2019).
- [15] M. A. Silaev, *Phys. Rev. B* **102**, 180502(R) (2020).
- [16] H. T. Simensen, L. G. Johnsen, J. Linder, and A. Brataas, *Phys. Rev. B* **103**, 024524 (2021).
- [17] M. Tanhayi Ahari and Y. Tserkovnyak, *Phys. Rev. B* **103**, L100406 (2021).
- [18] Y. Ominato, A. Yamakage, and M. Matsuo, *Phys. Rev. B* **106**, L161406 (2022).
- [19] R. Ojajarvi, F. S. Bergeret, M. A. Silaev, and T. T. Heikkilä, *Phys. Rev. Lett.* **128**, 167701 (2022).
- [20] C. Sun and J. Linder, *Phys. Rev. B* **107**, 144504 (2023).
- [21] X. Montiel and M. Eschrig, *Phys. Rev. B* **107**, 094513 (2023).
- [22] K. D. Usadel, *Phys. Rev. Lett.* **25**, 507 (1970).
- [23] J. W. Serene and D. Rainer, *Phys. Rep.* **101**, 221 (1983).
- [24] G. Eilenberger, *Z. Phys.* **214**, 195 (1968).
- [25] J. Rammer and H. Smith, *Rev. Mod. Phys.* **58**, 323 (1986).
- [26] A. Cottet, D. Huertas-Hernando, W. Belzig, and Y. V. Nazarov, *Phys. Rev. B* **80**, 184511 (2009).
- [27] J. A. Ouassou, A. Pal, M. Blamire, M. Eschrig, and J. Linder, *Sci. Rep.* **7**, 1932 (2017).
- [28] M. Amundsen and J. Linder, *Phys. Rev. B* **100**, 064502 (2019).
- [29] J. Linder and M. Amundsen, *Phys. Rev. B* **105**, 064506 (2022).
- [30] W. Belzig, F. K. Wilhelm, C. Bruder, G. Schön, and A. D. Zaikin, *Superlattices Microstruct.* **25**, 1251 (1999).
- [31] M. Eschrig, *Rep. Prog. Phys.* **78**, 104501 (2015).
- [32] N. Schopohl and K. Maki, *Phys. Rev. B* **52**, 490 (1995).
- [33] N. Schopohl, *arXiv:cond-mat/9804064*.
- [34] A. Konstandin, J. Kopu, and M. Eschrig, *Phys. Rev. B* **72**, 140501(R) (2005).
- [35] S. H. Jacobsen, J. A. Ouassou, and J. Linder, *Phys. Rev. B* **92**, 024510 (2015).
- [36] M. Y. Kuprianov and V. F. Lukichev, *Zh. Eksp. Teor. Fiz* **94**, 149 (1988).
- [37] F. S. Bergeret, A. F. Volkov, and K. B. Efetov, *Rev. Mod. Phys.* **77**, 1321 (2005).
- [38] P. Virtanen, R. Gommers, T. E. Oliphant, M. Haberland, T. Reddy, D. Cournapeau, E. Burovski, P. Peterson, W. Weckesser,

- J. Bright, S. J. van der Walt, M. Brett, J. Wilson, K. J. Millman, N. Mayorov, A. R. J. Nelson, E. Jones, R. Kern, E. Larson, C. J. Carey *et al.*, [Nat. Methods](#) **17**, 261 (2020).
- [39] J. A. Ouassou, S. H. Jacobsen, and J. Linder, [Phys. Rev. B](#) **96**, 094505 (2017).
- [40] R. C. Dynes, V. Narayanamurti, and J. P. Garno, [Phys. Rev. Lett.](#) **41**, 1509 (1978).
- [41] K. Senapati, M. G. Blamire, and Z. H. Barber, [Nat. Mater.](#) **10**, 849 (2011).
- [42] I. Gomperud and J. Linder, [Phys. Rev. B](#) **92**, 035416 (2015).